Published in final edited form as:

Biomaterials. 2015 December ; 72: 138–151. doi:10.1016/j.biomaterials.2015.08.050.

Controlled Dual Delivery of Fibroblast Growth Factor-2 and Interleukin-10 by Heparin-based Coacervate Synergistically Enhances Ischemic Heart Repair

William C.W. Chen[1,2,†], **Brandon G. Lee**[1,*], **Dae Woo Park**[3,4,*], **Kyobum Kim**[1,5], **Hunghao Chu**[1], **Kang Kim**[1,3,4,6], **Johnny Huard**[2,6,‡], and **Yadong Wang**[1,6,7,8,§]

[1]Department of Bioengineering, Swanson School of Engineering, University of Pittsburgh, Pittsburgh, PA, USA 15261

[2]Stem Cell Research Center, Department of Orthopaedic Surgery, School of Medicine, University of Pittsburgh, Pittsburgh, PA, USA 15219

[3]Center for Ultrasound Molecular Imaging and Therapeutics, Department of Medicine, University of Pittsburgh School of Medicine, PA, USA 15260

[4]Heart and Vascular Institute, University of Pittsburgh Medical Center (UPMC), Pittsburgh, PA, USA 15213

[5]Division of Bioengineering, College of Life Sciences and Bioengineering, Incheon National University, Incheon, Korea

[6]McGowan Institute for Regenerative Medicine, University of Pittsburgh, PA, USA 15219

[7]Department of Surgery, School of Medicine, University of Pittsburgh, Pittsburgh, PA, USA 15260

[8]Department of Chemical and Petroleum Engineering, Swanson School of Engineering, University of Pittsburgh, Pittsburgh, PA, USA 15261

[§]Corresponding Author: Yadong Wang, Ph.D., Biomaterials Foundry, Department of Bioengineering, University of Pittsburgh, 3700 O'Hara Street, Pittsburgh, PA 15261, Tel: 1-412-624-7196, yaw20@pitt.edu.

[†]Current address: Research Laboratory of Electronics and Department of Biological Engineering, Massachusetts Institute of Technology, Cambridge, MA, USA 02139

[‡]Current address: Department of Orthopaedic Surgery, Medical School, University of Texas Health Science Center at Houston, Houston, TX, USA 77030; Regenerative and Translational Medicine Institute, Steadman Philippon Research Institute, Vail, CO, USA 81657

[*]These authors contributed equally to the current study

Authorship Contributions:

W.C. conceptualized and designed research, performed experiments, analyzed data, and wrote the manuscript; B.G.L. and D.W.P. performed experiments and analyzed data; K.B.K. prepared materials, performed experiments, and analyzed data; H.C. conceptualized research and prepared materials; K.K. designed research, analyzed data, and provided lab space and equipment; J.H. designed research, provided equipment and funding, and edited the manuscript; Y.W. conceptualized and designed research, provided equipment and funding, edited and approved the manuscript.

Disclosure of Conflicts of Interest

J.H. received remuneration from Cook MyoSite, Inc. for consulting services and for royalties received from technology licensing during the period that the above research was performed. All other authors have no conflict of interest to disclose.

Abstract

Myocardial infarction (MI) causes myocardial necrosis, triggers chronic inflammatory responses, and leads to pathological remodeling. Controlled delivery of a combination of angiogenic and immunoregulatory proteins may be a promising therapeutic approach for MI. We investigated the bioactivity and therapeutic potential of an injectable, heparin-based coacervate co-delivering an angiogenic factor, fibroblast growth factor-2 (FGF2), and an anti-inflammatory cytokine, Interleukin-10 (IL-10) in a spatially and temporally controlled manner. Coacervate delivery of FGF2 and IL-10 preserved their bioactivities on cardiac stromal cell proliferation *in vitro*. Upon intramyocardial injection into a mouse MI model, echocardiography revealed that FGF2/IL-10 coacervate treated groups showed significantly improved long-term LV contractile function and ameliorated LV dilatation. FGF2/IL-10 coacervate substantially augmented LV myocardial elasticity. Additionally, FGF2/IL-10 coacervate notably enhanced long-term revascularization, especially at the infarct area. In addition, coacervate loaded with 500 ng FGF2 and 500 ng IL-10 significantly reduced LV fibrosis, considerably preserved infarct wall thickness, and markedly inhibited chronic inflammation at the infarct area. These results indicate that FGF2/IL-10 coacervate has notably greater therapeutic potential than coacervate containing only FGF2. Overall, our data suggest therapeutically synergistic effects of FGF-2/IL-10 coacervate, particularly coacervate with FGF2 and 500 ng IL-10, for the treatment of ischemic heart disease.

Keywords

controlled release; angiogenesis; anti-inflammation; myocardial infarction; coacervate; fibroblast growth factor-2; Interleukin-10

Introduction

Coronary heart disease (CHD) affects 15.4 million Americans and is the most common type of heart disease. CHD alone accounts for 385,000 deaths and costs an estimated total of $108.9 billion annually (direct and indirect) in the United States [1]. CHD caused by pathological blockage of the coronary circulation may lead to prolonged ischemia which in turn results in permanent cardiomyopathy and/or myocardial infarction (MI) [2]. MI causes death of cardiac myocytes and triggers local inflammatory responses and the compensatory scar formation, leading to pathological remodeling and ultimately heart failure (HF) [2]. Recent experimental therapies for cardiac repair primarily focus on revascularization and regeneration of impaired myocardium [3–5]. However, to break the vicious cycle of MI-to-HF, it is critical to not only promote revascularization of the ischemic tissue but also modulate the over-activated and prolonged inflammation following myocardial injury [6].

Our research team has recently developed a controlled delivery system that utilizes the charge interaction between a biodegradable polycation, poly(ethylene argininylaspartate diglyceride) (PEAD), and a natural polyanion, heparin, to form coacervate. This heparin-based coacervate delivery platform protects and steadily releases heparin-binding growth factors, including fibroblast growth factor-2 (FGF2) [7], nerve growth factor (NGF) [7], heparin-binding epidermal growth factor-like growth factor (HB-EGF) [8], stromal cell-derived factor (SDF)-1α [9], and bone morphogenetic protein-2 [10]. In addition, heparin-

based coacervate has been shown to efficiently deliver HB-EGF in a mouse model of skin wound healing, accelerating keratinocyte migration and wound closure [8], and FGF2 in a mouse model of subcutaneous injection, promoting local neoangiogenesis and blood vessel maturation [11]. Furthermore, in a murine MI model, coacervate containing 500 ng FGF2 has been proven effective in augmenting functional angiogenesis and blood vessel stabilization, reducing cardiomyocyte death and peri-infarct fibrosis, and improving cardiac function [12]. Utilizing the versatile protein-binding capacity of heparin, we theorized that dual delivery of FGF2 and an anti-inflammatory agent by coacervate can be therapeutically more effective than the delivery of FGF2 alone.

Interleukin-10 (IL-10) is a pleiotropic cytokine that exhibits broad immunoregulatory and anti-inflammatory activities [13]. Human IL-10 binds to heparin with high affinity at pH 7.4 (K_d=54 ± 7 nM) [14]. The role of IL-10 in the cardiac milieu has been investigated in recent years [15]. In congestive HF patients, higher plasma levels of anti-inflammatory mediators such as IL-10 notably correlates with augmented contractile function of the left ventricle (LV) [16]. Daily subcutaneous injections of recombinant human IL-10 (rhIL-10, 75 μg/kg-day) for 4 weeks in a rat model of acute MI (AMI) resulted in significantly reduced productions of proinflammatory cytokines, diminished myocardial macrophage infiltration, and augmented LV function [17]. Nonetheless, due to its short half-life (2.7 to 4.5 hours) after subcutaneous injection [18], it typically requires repeated administrations of high-dose IL-10 to achieve therapeutic potency, leading to increasing risks of side-effects and high treatment cost. Given its high heparin-binding affinity, coacervate may serve as an ideal vehicle for sustained, localized delivery of IL-10 and further reduce the required therapeutic dosage.

Controlled co-delivery of two trophic factors to promote tissue repair has lately been explored [19–23]. In particular, sustained delivery of FGF2 and hepatocyte growth factor (HGF) via cross-linked albumin-alginate microcapsules augmented angiogenic and arteriogenic responses, improved cardiac perfusion and function, and attenuated cardiac hypertrophy and fibrosis [21]. Co-delivery of angiogenic FGF-2 and arteriogenic platelet-derived growth factor (PDGF)-BB with self-assembling peptides resulted in reduced infarct size, stable vessel formation, and improvement of cardiac function [22]. Using a poly(D,L-lactic-co-glycolic acid) microsphere/alginate hydrogel hybrid system, combined delivery of vascular endothelial growth factor (VEGF) and angiopoietin-1 synergistically enhanced vascular maturation and attenuated muscle degeneration at the ischemic site in an murine model hind-limb ischemia, more effective than single factor delivery [23]. On the other hand, our group recently demonstrated that heparin-based coacervate is capable of incorporating and sustaining the release of VEGF and HGF for at least three weeks [24]. Dual delivery of VEGF and HGF by coacervate showed stronger angiogenic effects on endothelial cell proliferation and tube formation *in vitro* than free or coacervate delivery of individual factor [24]. Consequently, we hypothesize that dual delivery of FGF2 and IL-10 synergistically enhances their angiogenic and/or cardioprotective potency in the ischemic heart.

In the present study, we characterized FGF2/IL-10 coacervate and investigated its bioactivity on cardiac stromal cells *in vitro*. The therapeutic efficacy of FGF2/IL-10

coacervate was evaluated in a mouse AMI model. Our data suggest that controlled release of FGF2 and IL-10 by heparin-based coacervate exerts synergistic effects in improving long-term cardiac function, augmenting myocardial elasticity, promoting revascularization, ameliorating myocardial fibrosis, and inhibiting chronic inflammation.

Material and Methods

Preparation of FGF-2/IL-10 Coacervate

Poly(ethylene argininylaspartate diglyceride) (PEAD) was synthesized as previously described [7, 25]. PEAD and clinical-grade heparin (Scientific Protein Labs, Waunakee, WI, USA) were separately dissolved in 0.9% normal saline (Baxter Healthcare, Deerfield, IL, USA) at 10 mg ml^{-1} and sterilized by passing through 0.22 μm syringe filter. A 5:1 ratio of PEAD and heparin by weight was used to maintain electric neutrality as previously described [7]. Heparin was first complexed with a pre-determined, equal amount of recombinant human FGF-2 (rhFGF-2; 17.2 kDa protein consisting of 154 amino acid residues) and IL-10 (rhIL-10; 18.6 kDa protein of consisting of 161 amino acid residues) (both from PeproTech, Rocky Hill, NJ, USA) and mixed well. PEAD was subsequently added into the solution containing [heparin:FGF-2/IL-10] complexes. Self-assembly of PEAD and [heparin:FGF-2/IL-10] immediately precipitated the ternary complex out of solution to form the FGF-2/IL-10 coacervate. Precipitation of coacervate complexes immediately increased opaque turbidity in solution. Coacervate was freshly prepared immediately before all *in vitro* and *in vivo* experiments to avoid aggregation. Coacervate droplet size was measured by Zetasizer Nano ZS90 (Malvern, Worcestershire, UK) and reported as the mean with polydispersity index (PDI) from 25 measurements. Results were then averaged from measurements of three independent coacervate samples. PDI in the area of light scattering depicts the droplet size distribution.

Fluorescent labeling of FGF-2/IL-10 Coacervate

To fluorescently visualize the incorporation of FGF2 and IL-10 in coacervate complexes, amine-reactive dyes (Thermo Scientific, Waltham, MA, USA) were utilized to label FGF2 and IL-10 molecules, following the manufacturer's instructions. Briefly, FGF2 and IL-10 solutions were added into vials containing concentrated NHS ester-activated derivatives of DyLight 488 and DyLight 594 respectively and reacted at room temperature for 1 hour. A spin desalting column was used to remove unreacted dyes. To triply label biological components in FGF-2/IL-10 coacervate, FGF2 and IL10 were first labelled with NHS-DyLight 488 and NHS-DyLight 405 individually. FGF2-DL488 and IL-10-DL405 were then mixed well with heparin before rhodamine conjugated *ulex europaeus* agglutinin I (UEA-1) was applied to label heparin. PEAD was then added into the solution containing [heparin-rhodamine: FGF2-DL488/IL-10-DL405] complexes to form coacervate.

In vitro Release Profile of FGF-2/IL-10 Coacervate

The release profile of FGF2/IL-10 coacervate was determined *in vitro* as previously described [7, 24]. Briefly, FGF2/IL-10 coacervate was freshly prepared with a mass ratio of PEAD:heparin:FGF2:IL-10=500:100:1:1, using 100 ng each of FGF2 and IL-10. To simulate release of cargo molecules *in vivo*, additional phosphate-buffered saline (PBS)

supplemented with 0.5 U/mL heparinase II was added to each sample to bring up the final volume to 200 μL. Four independent samples were then placed statically in a humidified cell culture incubator at 37 °C . At Day 0, 0.5, 1, 4, 7, 10, 14, and 21, samples were pelleted by centrifugation (12,100 g for 10 min), followed by the collection of supernatants. Samples were then replenished with fresh solution and well mixed before being returned to the incubator. Solutions were stored at −80°C for future analysis. After the final collection on Day 21, samples were replenished with PBS supplemented with 2 U/mL heparinase II and incubated at 37 °C overnight in order to dissociate the remaining coacervate. The amount of FGF2 and IL-10 released into the supernatant was quantified by enzyme-linked immunosorbent assay (ELISA) for FGF2 or IL-10 respectively (both from Abcam, Cambridge, MA, USA), following the manufacturer's instructions. Supernatants collected from four samples at all-time points were analyzed simultaneously. The absorbance was recorded by SynergyMX (Biotek, Winooski, VT, USA) or Infinite 200 PRO plate reader (Tecan, Männedorf, Switzerland). Results were averaged. The loading efficiency was determined from the first collection immediately after the initial resuspension (Day 0).

Primary Cell Isolation and Culture

Single donor-derived human umbilical vein endothelial cells (HUVECs) and human cardiac fibroblasts (hCFs) were purchased from Lonza (Allendale, NJ, USA) and respectively expanded in complete endothelial cell growth medium 2 (EGM-2, Lonza) and DMEM high glucose supplemented with 10% fetal bovine serum (FBS) and 1% penicillin-streptomycin (P/S) (all from Life Technologies, Grand Island, NY, USA). Mouse cardiac fibroblasts (mCFs) were isolated as previously described [26] and expanded in DMEM high glucose with 10% FBS and 1% P/S. Human heart pericytes (hHPs) were isolated and purified by flow cytometry as we previously reported [27], in compliance with the Institutional Review Board protocol 0506176 at the University of Pittsburgh. hHPs were expanded in DMEM high glucose with 20% FBS and 1% P/S. Primary cells at passage 5–7 were used in subsequent experiments.

Measurement of Cell Proliferation *in vitro*

HUVECs, hCFs, hHPs, and mCFs were trypsinized and plated in triplicate (1.5×10^3 cells/well) overnight with 100 μl complete culture media in bottom wells of a HTS transwell-96 well permeable support system (Corning, Tewksbury, MA, USA). Immediately before the transwell support was assembled, all bottom wells were first filled up with 135 μl fresh serum-free basal media (EBM-2 for HUVECs and DMEM for hCFs, hHPs, and mCFs; both supplemented with 1% P/S) with or without 10 ng/ml (for HUVECs) or 100 ng/ml (for all other cell types) of tumor necrosis factor alpha (TNF-α). Free 500 ng FGF2 combined with either 100 ng or 500 ng IL-10 and coacervate containing a fixed load of 500 ng FGF2 alone or combined with either 100 ng or 500 ng IL-10 were resuspended in 75 μl serum-free basal media and then added into transwells. Control transwells were added with plain basal media with or without empty coacervate vehicle. The final concentration of serum was approximately 33% of that in complete culture media in each well. Plates were assembled and subsequently incubated for 72 hours under ambient conditions. After washing all wells, CellTiter 96® AQueous One Solution Cell Proliferation Assay (MTS) reagent (Promega, Madison, WI, USA) in DMEM was added. The plate was incubated in 5% CO_2 at 37 °C for

3 hrs, at which point the absorbance at 490 nm (with reference at 650 nm) was read with Infinite 200 PRO plate reader (Tecan, Männedorf, Switzerland). All experiments were independently repeated 3 times. Results were individually normalized to each experimental control and then averaged.

Experimental Animals

The Institutional Animal Care and Use Committee at the University of Pittsburgh approved the animal usage and surgical procedures performed in this study (Protocol 12010140). A Total of 77 male BALB/cJ mice at 9–12 weeks old (Jackson Laboratory, Bar harbor, ME, USA) were used for this study.

Intramyocardial Administration of FGF-2/IL-10 Coacervate in a Mouse Model of Acute Myocardial Infarction (AMI)

After the induction of anesthesia with 4% isoflurane gas, mice were intubated and inhalationally anesthetized with 2% isoflurane gas throughout the surgery. The induction of myocardial infarction (MI) and intramyocardial injection have been performed as we previously reported [12, 28]. In brief, MI was microscopically induced by permanent ligation of the left anterior descending coronary artery (LAD). Mice were then randomly assigned to one of the five groups: saline control, FGF2 500 ng coacervate (Coa-F-500), Free FGF2/IL-10 500/500 ng (Free-F/I-500/500), FGF2/IL-10 500/100 ng coacervate (Coa-F/I-500/100), or FGF2/IL-10 500/500 ng coacervate (Coa-F/I-500/500). Five minutes after the induction of MI, free or coacervate FGF2/IL-10 diluted in 30 μl of sterile 0.9% normal saline were injected at three sites of the ischemic myocardium (center and two borders of the infarct). Control mice received injections of 30 μl saline.

Echocardiography

Echocardiographic studies were performed repeatedly before surgery and at 5 days, 2 and 6 weeks post-surgery to assess the cardiac function as we previously described [12, 28]. Briefly, mice were anesthetized with 2% isoflurane gas and immobilized on a heated stage equipped with electrocardiography. Heart and respiratory rates were continuously monitored while the body temperature was maintained at 37°C. Echocardiographic parameters were measured using a high-resolution echocardiography system (Vevo 2100) equipped with a high-frequency linear probe (MS400, 30 MHz) (FUJIFILM VisualSonics, Toronto, Ontario, Canada). Three hundred B-mode frames were acquired at a frame rate of 40 Hz during each scan. End-systolic dimension (ESD) and end-diastolic dimensions (EDD) were determined from the short axis images of the LV and measured from 10 consecutive beats using the M-mode tracing. End-systolic area (ESA) and end-diastolic area (EDA) were measured from short-axis images of the LV. All echocardiographic measurements were taken at the mid-infarct level in LV. Functional parameters, including LV fractional shortening (LVFS), LV fractional area change (LVFAC), and LV ejection fraction (LVEF), were determined as previously described [29–31]. Mice died or sacrificed for histological analysis prior to 6 weeks post-injection were not included in the echocardiographic study.

Ultrasonic Analysis of Myocardial Elasticity

The ultrasound in-phase and quadrature (IQ) data were separately acquired at 6 weeks post-MI during the echocardiographic scanning described in the above section (N=3 per group). The IQ data were then converted to the radio frequency (RF) data using standard quadrature sampling algorithms and subsequently analyzed by a blinded investigator. Briefly, pixels were selected in the lateral (infarcted region) and anterior medial (non-infarct region) walls of LV in the first B-mode frame. The 2D phase-sensitive speckle tracking was then applied to the RF data to obtain frame-to-frame axial displacements (direction along the ultrasound beam) of the selected pixels [32, 33]. Axial displacements were accumulated during each cardiac cycle (from diastole to systole). Axial strains in LV wall were obtained by derivative of the accumulated axial displacements. To unbiasedly estimate myocardial elasticity, two regions of interest (ROI) in the axial strain map were respectively selected in the infarcted and non-infarct LV walls. Axial strains in these ROIs were spatially averaged and then normalized by dividing the averaged strain of the infarcted ROI by that of the non-infarct ROI.

Histology and Immunohistochemistry

Mice were sacrificed at 6 weeks post-surgery. Intraventricular injection of 1M potassium chloride (KCl) was performed to arrest hearts in diastole. For histology and immunohistochemistry, harvested hearts were flash frozen in 2-methylbutane (Sigma-Aldrich, St. Louis, MO, USA) pre-cooled in liquid nitrogen, preserved at −80°C, and then processed as formerly described [12, 28]. Briefly, frozen hearts were serially cryosectioned at 6–8 μm thickness from apex to the ligation level (approximately 0.5 mm in length). Each series contained 18–21 heart sections and was collected on one glass slide. Hematoxylin and eosin (H&E) staining was performed following the standard protocol. For immunohistochemistry, sections were fixed in a pre-cooled (−20°C) mixture of methanol and acetone (1:1) for 5 min or in 4% paraformaldehyde for 8 min prior to staining. Non-specific antibody binding was blocked with 10% donkey or goat serum for 1–2 hours at room temperature (RT), and, if necessary, with the Mouse-on-Mouse antibody staining kit (Vector Laboratories, Burlingame, CA, USA). Sections were incubated overnight at 4 °C with the following primary antibodies (all diluted with 5% donkey or goat serum in PBS): rat anti-mouse CD31 antibody (diluted at 1:100; Becton-Dickinson Biosciences, Franklin Lakes, NJ, USA), mouse anti-mammalian alpha-smooth muscle actin (αSMA)-FITC (diluted at 1:100; Sigma-Aldrich, St. Louis, MO, USA), and/or rat anti-mouse CD68 antibody (diluted at 1:200; Abcam, Cambridge, MA, USA). Sections were then incubated at RT for 1 hour with the following fluorochrome-conjugated antibodies: donkey anti-rat-Alexa594 IgG or goat anti-rat-Alexa488 IgG (both diluted at 1:250; Jackson Laboratory, Bar Harbor, ME, USA). Nuclei were stained with 4’,6-diamidino-2-phenylindole (DAPI) (1:1000, Life Technologies, Grand Island, NY, USA) at RT for 5 min. Immunofluorescent images were taken by Nikon Eclipse Ti fluorescence microscope equipped with NIS-Elements AR imaging software (both from Nikon, Tokyo, Japan).

Measurement of Cardiac Fibrosis and Infarct Wall Thickness

Masson's trichrome staining kit (IMEB, San Marcos, CA, USA) was used to reveal collagen deposition on heart serial cross-sections, following the manufacturer's instruction. The area of collagen deposition (representing fibrosis/scar) and the area of the entire left ventricular cardiac tissue (including septal area but excluding right ventricle and void space in the chamber cavity) were separately measured using a digital image analyzer (Image J, National Institutes of Health, Bethesda, MD, USA). Fibrotic area fraction was estimated as the ratio of left ventricular fibrotic tissue to the entire left ventricular tissue. Results were averaged from 6 randomly selected sections at comparable infarct levels per heart. Left ventricular wall thickness at the center of the infarct was estimated as the mean of 3 adjacent measurements (0.25 mm apart) and was averaged from 6 randomly selected sections at comparable infarct levels per heart.

Quantification of Chronic Inflammation and Revascularization

To evaluate chronic inflammation within the infarct region, immunofluorescent staining of phagocytic cell marker CD68 was performed on serial cryosections as described above. The infiltration index, represented by the number of CD68+ phagocytic cells per mm^2, was subsequently computed by a blinded investigator from 6–8 randomly selected images of the infarct region of each heart at the mid-infarct level, using Image J. To quantify revascularization post-MI, immunofluorescent staining of endothelial cell (EC) marker CD31 and vascular smooth muscle cell (VSMC) marker αSMA was sequentially performed on serial cryosections. The capillary density, represented by the number of CD31+ capillary ECs per mm^2, was subsequently computed by a blinded investigator from 6 randomly selected images of the infarct or peri-infarct area of each heart at the mid-infarct level, using Image J as described previously [12, 28]. The VSMC density, represented by the number of perivascular (i.e. adjacent to CD31+ ECs and/or surrounding vascular structures) αSMA+ cells per mm^2, was subsequently computed from 6 randomly selected images of the infarct region or peri-infarct area of each heart at the mid-infarct level, using Image J.

Multi-photon Excitation Imaging

For multi-photon excitation (MPE) imaging, rhodamine tagged with UEA-1 (2 μg) was mixed well with heparin before PEAD was added into the solution containing [heparin:rhodamine] complexes to form coacervate. Intramyocardial injection of free or heparin-bound rhodamine-UEA-1 (2 μg) or rhodamine-UEA-1 coacervate (all diluted in 30 μl of sterile 0.9% normal saline) was performed after the induction of MI as described above. Hearts were harvested at 5, 14, and 28 days post-injection, washed 3 times in PBS, and immediately fixed in fresh 4% paraformaldehyde overnight. Hearts were then washed in PBS twice and subsequently immersed in ScaleView-A2 optical clearing agent (Olympus Scientific Solutions Americas, Waltham, MA, USA) at 4°C for 7–10 days. Processed hearts were block-sectioned at 1 mm thickness to obtain cross-sections from apex to ligature immediately before performing MPE imaging on an Olympus multiphoton microscope at the Center for Biologic Imaging, University of Pittsburgh.

Statistical Analysis

All measured data are presented as mean ± standard deviation (SD). Kaplan-Meier survival curve estimation with log-rank test was performed to compare the animal survival rate between treatment groups. Statistical differences between groups were analyzed by one-way ANOVA (multiple groups) or two-way repeated ANOVA (for repeated echocardiographic measurements) with 95% confidence interval. Statistical significance was set at $p \leqq 0.05$. Bonferroni multiple comparison test was performed for ANOVA post-hoc analysis. Statistical analyses were performed with SigmaStat 3.5 (Systat Software) and SPSS21 (IBM) statistics software.

Results

Characterization of FGF-2/IL-10 coacervate

FGF-2 and IL-10 both have high heparin-binding affinity (FGF-2: $K_d \approx 74$ nM [34]; IL-10: $K_d \approx 54$ nM [14]). A mixture of FGF2 and IL-10 is first complexed with heparin and subsequently incorporated into the ternary [PEAD:heparin:FGF2/IL-10] coacervate droplets by adding PEAD. We have theorized that the four structural components of FGF-2/IL-10 coacervate (PEAD, heparin, FGF2, and IL-10) are evenly distributed when the coacervate forms, following affinity-based binding of FGF2 and IL-10 to heparin, charge interactions between PEAD and heparin, and physical entrapment of FGF2 and IL-10 within the complex coacervate (Figure 1A). FGF2/IL-10 coacervate droplets had an average size of 432.6 ± 42.1 nm in diameter, smaller than the sizes of coacervate droplets containing only FGF2 (608.3 ± 96.3 nm) or IL-10 (502.6 ± 101.5 nm) (Figure 1B).

To simulate the release of cargo proteins *in vivo*, the amount of FGF2 and IL-10 released from FGF2/IL-10 coacervate was measured by ELISA after immersion in PBS supplemented with heparinase II (0.5 U/mL) for 0, 0.5, 1, 4, 7, 10, 14, and 21 days (N=4). The loading efficiency of FGF2 and IL-10 was approximately 98.0 ± 1.6% and 97.9 ± 0.5% respectively (Figure 1C). Cumulatively, FGF2/IL-10 coacervate released roughly 16.1 ± 3.8% and 12.5 ± 2.4% FGF2 and IL-10 respectively during the first 12 hours and approximately 28.7 ± 5.0% and 14.8 ± 2.3% respectively by 24 hours (Figure 1C). The total release of FGF2 and IL-10 from coacervate was estimated to be 86.8 ± 7.1% and 28.2 ± 3.6% respectively over the 21-day duration (Figure 1C). Final digestion with 2 U/mL heparinase II showed that at least nearly 3% FGF2 and 15% IL-10 remained in residual coacervate. However, these data did not take into account the spontaneous degradation of free IL-10, on average 1.59% per day, in PBS supplemented with 0.5 U/mL heparinase II (Supplemental Figure 1).

To further demonstrate that FGF2 and IL-10 have been evenly incorporated into coacervate droplets, we fluorescently labeled FGF2 (DyLight 488, green) and IL-10 (DyLight 594, red). Spherical droplets of different sizes containing FGF-2 and IL-10 were observed following coacervate formation (Figure 1D). High-magnification confocal microscopy showed an even distribution of FGF-2 and IL-10 molecules within a coacervate droplet (Figure 1E). By triply labeling heparin (rhodamine, red), FGF2 (DyLight 488, green) and IL-10 (DyLight

405, blue), the nearly homogeneous structure of FGF-2/IL-10 coacervate was further revealed (Figure 1F).

Bioactivity of FGF-2/IL-10 coacervate *in vitro*

The bioactivity of FGF2/IL-10 coacervate on cardiac stromal cell proliferation was tested in a non-contact release system to avoid direct ingestion of coacervate particles by cells. Cells were cultured at bottom wells with treatment solutions in suspended transwells. Human umbilical vein endothelial cells (HUVECs), human cardiac fibroblasts (hCFs), and human heart pericytes (hHPs), and mouse cardiac fibroblasts (mCFs) were used in this assay. Cells were seeded in complete culture media overnight and then maintained in diluted media throughout the experiment to simulate nutrient starvation following coronary artery blockage. Based on our previous study [12], we selected a fixed load of FGF2 (500 ng) alone or combined with a low (100 ng) or high (500 ng) load of IL-10 for coacervate delivery (designated as Coa-F-500, Coa-F/I-500/100, and Coa-F/I-500/500 respectively). Free 500 ng FGF2 combined with either 100 ng or 500 ng IL-10 served as positive controls (designated as Free-F/I-500/100 and Free-F/I-500/500 respectively). No treatment (plain or DMEM basal medium) and empty coacervate vehicle groups served as negative controls.

After incubation for 72 hours, Free-F/I-500/100, Coa-F-500, Coa-F/I-500/100 and Coa-F/I-500/500 significantly increased HUVEC proliferation when compared with the no-treatment control and Free-F/I-500/500 (Figure 2A, all $p<0.01$). Coa-F/I-500/100 and Coa-F/I-500/500 showed trends of reducing hCF proliferation and notably inhibited mCF proliferation when compared with Free-F/I-500/100 and Free-F/I-500/500 (Figure 2A, both $p<0.05$). Coa-F/I-500/500 demonstrated the most significant inhibition of mCF proliferation when compared with the no-treatment control ($p=0.006$). On the other hand, Free-F/I-500/100, Free-F/I-500/500, and Coa-F/I-500/500 slightly promoted hHP proliferation (Figure 2A, all $p>0.05$). No significant difference was observed between no-treatment control and empty coacervate vehicle group in all four cell types (Figure 2A, $p>0.05$).

To further simulate inflammatory stress following ischemic insult, 10 ng/ml of TNF-α for HUVECs and 100 ng/ml of TNF-α for all other cell types were added into bottom wells immediately before the start of the experiment. After incubation for 72 hours, Coa-F-500, Coa-F/I-500/100 and Coa-F/I-500/500 significantly promoted HUVEC proliferation when compared with the no-treatment control (Figure 2B, all $p<0.05$). All three coacervate groups exhibited reduced hCF proliferation and significantly inhibited mCF proliferation when compared with the no-treatment control and Free-F/I-500/100 (Figure 2B, all $p<0.01$). Similarly, Coa-F/I-500/500 showed the most striking inhibition of mCF growth when compared with all non-coacervate groups (all $p<0.01$). All treatment groups maintained hHP growth under inflammatory stress (all $p>0.05$). There was no notable difference between no-treatment and empty vehicle groups under inflammatory stress in all tested cell populations (Figure 2B, $p>0.05$). Altogether these results suggest that FGF2/IL-10 coacervate supports HUVEC growth under nutrient deprivation while inhibiting the proliferation of CFs, especially under inflammatory stress.

Intramyocardial codelivery of FGF-2/IL-10 coacervate synergistically improves cardiac function

We selected 500 ng FGF2 combined with a low (100 ng) or high (500 ng) dose of IL-10 for coacervate-based codelivery (Coa-F/I-500/100 and Coa-F/I-500/500 respectively) and examined the therapeutic efficacy of FGF-2/IL-10 coacervate *in vivo*. Intramyocardial injection of saline, coacervate containing only 500 ng FGF2 (Coa-F-500), or free FGF-2 500 ng combined with free IL-10 500 ng (Free-F/I-500/500) served as controls. The mortality rate was around 15% during and immediately after the surgery. Among all mice which recovered from the surgery, two died in each of the following groups: Saline, Free-F/I-500/500, and Coa-F-500, and one died in each of the following groups: Coa-F/I-500/100 and Coa-F/I-500/500, before the terminal time point. Most of these deaths occurred within the first week post-surgery. These mice were excluded from functional studies. No significant difference in animal survival rate was noted.

Cardiac function was assessed by M- and B-mode echocardiography performed repeatedly at the mid-infarct level before (baseline) and after surgery at 5 days, 2 weeks, and 6 weeks (N=8 per group except Free-F/I-500/500, N=7; data analyzed by two-way repeated ANOVA). By analyzing the treatment effect, both FGF2/IL-10 coacervate groups exhibited substantially higher LVFS (Figure 3A), LVFAC (Figure 3B), and LVEF (Figure 3C) than Saline (all $p<0.001$) and Free-F/I-500/500 (all $p<0.05$), indicating better LV contractility following controlled release of FGF2 and IL-10. However, only Coa-F/I-500/500, but not Coa-F/I-500/100, showed significant improvement in all three contractile parameters when compared with Coa-F-500 (all $p<0.005$). Moreover, Coa-F/I-500/500 had significantly better LVFAC and LVEF than Coa-F/I-500/100 (both $p<0.05$), suggesting a role of IL-10 dosage in prompting a notable synergistic effect for LV contractility.

In addition, ischemic hearts treated with either Coa-F/I-500/100 or Coa-F/I-500/500 had markedly reduced LVEDA (Figure 3D) and LVESA (Figure 3E) than Saline (all $p<0.001$) and Free-F/I-500/500 (all $p<0.005$), suggesting amelioration of progressive LV dilatation by FGF2/IL-10 coacervate treatment. Similarly, only Coa-F/I-500/500, but not Coa-F/I-500/100, showed significant diminution in both dilatation parameters when compared with Coa-F-500 (all $p<0.001$), suggesting a role of IL-10 dosage in ameliorating LV remodeling. All measurements of dimensional and functional echocardiographic parameters are listed in Supplemental Table T1. Overall, our results indicate that the intramyocardial administration of FGF2/IL-10 coacervate, regardless of the IL-10 dose, significantly improved the LV contractile function and reduced the LV dilatation. These data further suggest the importance of IL-10 dosage in the synergistic therapeutic effect induced by FGF2/IL-10 coacervate.

FGF-2/IL-10 coacervate amends elasticity of the infarcted myocardium

To further assess the effect of FGF2/IL-10 coacervate on myocardial elasticity, we performed ultrasonic strain estimation at 6 weeks post-MI. The axial strains were determined in the infarcted (area B) and non-infarct (area A) LV walls during a cardiac cycle using the 2D correlation based speckle tracking. Figure 4A shows the axial strain maps of normal (left panel) and untreated MI control (right panel) hearts laid over B-mode images

reconstructed from IQ data respectively (negative strains in blue color and positive strains in red). The elasticity of the infarcted myocardium was estimated from spatially averaged axial strains in B and subsequently normalized by dividing the averaged strain of B by that of A (B/A) (Figure 4A). B-mode images of normal and untreated MI control hearts without strain maps and ROIs are included in Supplemental Figure 2 for comparison. While all groups had similar averaged axial strains in A, Coa-F-500 (both $p<0.01$), Coa-F/I-500/100 (both $p<0.001$), and Coa-F/I-500/500 (both $p<0.001$) had significantly greater normalized strains than the saline control and Free-F/I-500/500 (Figure 4B, N=3 per group). Free-F/I-500/500 also exhibited notably higher normalized strains than the saline control ($p=0.004$) (Figure 4B). No significant difference was observed between the three coacervate treatment groups (Figure 4B, all $p>0.05$). These data indicate the efficacy of FGF2/IL-10 coacervate in sustaining the long-term LV myocardial elasticity.

FGF-2/IL-10 coacervate promotes long-term revascularization

The potency of intramyocardial administration of FGF2/IL-10 coacervate on long-term revascularization was investigated. Immunohistochemistry revealed the presence of CD31+ endothelial cells (ECs; mostly located at microvasculature/capillary) (Figure 5A) and vascular smooth muscle cells (VSMC; mostly surrounding larger blood vessels) (Figure 5A) in the infarct and peri-infarct areas at 6 weeks post-infarction. The number of CD31+ ECs was subsequently quantified in the infarct (Figure 5B) and peri-infarct (Figure 5C) areas (N=4 per group). Within the infarct area, Coa-F/I-500/500 had higher CD31+ EC density when compared with the saline control ($p<0.001$), Free-F/I-500/500 ($p=0.02$), and Coa-F-500 ($p>0.05$) (Figure 5B). Coa-F/I-500/100 had higher CD31+ EC density when compared with the saline control ($p=0.007$) and Free-F/I-500/500 ($p>0.05$) (Figure 5B). Within the peri-infarct area, Coa-F/I-500/500 exhibited the highest CD31+ EC density when compared with the saline control ($p<0.001$), Free-F/I-500/500 ($p<0.001$), Coa-F-500 ($p=0.001$), and Coa-F/I-500/100 ($p>0.05$) (Figure 5C). Coa-F/I-500/100 also had higher CD31+ EC density when compared with the saline control ($p=0.008$), Free-F/I-500/500 ($p=0.012$), and Coa-F-500 ($p>0.05$) (Figure 5C).

The number of VSMCs and/or pericytes (i.e. perivascular αSMA+ cells) was also quantified in the infarct (Figure 6A) and peri-infarct (Figure 6B) areas (N=4 per group) at 6 weeks post-infarction. The results showed that Coa-F/I-500/500 had significantly higher VSMC density when compared with the saline control ($p=0.008$), Free-F/I-500/500 ($p=0.038$), and Coa-F-500 ($p=0.031$) within the infarct area (Figure 6A). In addition, hearts treated with Coa-F/I-500/100 and Coa-F/I-500/500 exhibited trends of increased VSMCs within the peri-infarct area (Figure 6B). Altogether our results suggest FGF2/IL-10 coacervate treatment promotes long-term revascularization at 6 weeks post-infarction, especially with Coa-F/I-500/500 treatment. Additionally, these data imply that the revascularzing effect of FGF2/IL-10 coacervate is positively correlated with the dose of IL-10.

FGF-2/IL-10 coacervate reduces myocardial fibrosis

The effect of FGF2/IL-10 coacervate on long-term LV myocardial fibrosis was evaluated using Masson's trichrome histological staining (collagen deposition stained in blue/purple). At 6 weeks post-infarction, Coa-F/I-500/100 and Coa-F/I-500/500 appeared to have reduced

infarct size and scar formation at the mid-infarct level when compared with the saline control and Free-F/I-500/500 (Figure 7A). Quantitative analysis revealed that Coa-F/I-500/500 exhibited notably smaller LV scar fraction than the saline control (p=0.001) and all other treatment groups (all p>0.05) (Figure 7B, N=4 per group). Analysis of the LV wall thickness at the infarct center further showed that Coa-F/I-500/500 had a significantly thicker wall than the saline control (p<0.001) and all other test groups (all p<0.05) (Figure 7C, N=4 per group). These data suggest the efficacy of coacervate containing higher dose of IL-10 in ameliorating the formation of myocardial fibrosis and preserving wall thickness post-infarction.

FGF-2/IL-10 coacervate inhibits chronic phagocytic cell infiltration

To investigate the underlying mechanism for the amelioration of myocardial fibrosis, we examined the anti-inflammatory effect of FGF2/IL-10 coacervate. Phagocytic cells within the infarct area were detected by anti-CD68 immunohistochemistry at 6 weeks post-infarction (Figure 8A). All three coacervate groups showed significantly decreased numbers of infiltrated CD68+ phagocytic cells within the infarct area when compared with the saline control (Figure 8B, N=4 per group; Coa-F-500, p=0.037; Coa-F/I-500/100, p=0.007; Coa-F/I-500/500, p=0.002). In particular, Coa-F/I-500/100 and Coa-F/I-500/500 exhibited substantial 47.2% and 59.9% reduction of CD68+ cells respectively when compared with Free-F/I-500/500 (Figure 8B, both p>0.05). Although there is no statistical significance in the number of CD68+ cells between all three coacervate groups, comparing with Coa-F-500, Coa-F/I-500/100 and Coa-F/I-500/500 displayed notable 23.9% and 42.3% diminution of CD68+ cells respectively. Together these results suggest that coacervate delivery of FGF2 and IL-10 increases their long-term potency for immunoregulation, and the addition of IL-10 in FGF2 coacervate augments the inhibition of chronic inflammation.

Estimation of the duration of coacervate treatment *in vivo*

To estimate the duration of coacervate treatment post-MI, we employed multi-photon excitation (MPE) imaging to detect intramyocardially injected rhodamine-tagged coacervate (Coa-Rho). Collagen fibers were identified by second harmonic generation (SHG) signals. At 5 days after injection, Coa-Rho exhibited robust fluorescent signals within the infarct area while weak signals were detected in free (Free-Rho) or heparin-bound (Hep-Rho) rhodamine injected hearts (Figure 9A). At 2 and 4 weeks post-MI, fluorescent signals were only detected in hearts injected with Coa-Rho, but not with Free-Rho or Hep-Rho (Figure 9A). No signal was detected in any group at 6 weeks post-MI. Quantification of the fluorescence volume found that at 5 days post-injection, Coa-Rho had 28.9 ± 11.1 and 7.1 ± 2.7 folds higher signals than that of Free-Rho and Hep-Rho respectively (Figure 9B, N=3 per group, p<0.05). Moreover, when compared with the signal on Day 5, Coa-Rho had roughly 65.9% and 25.7% of residual fluorescence volume at 2 and 4 weeks post-injection respectively (Figure 9B, N=3 per time point). These results suggest a temporal distribution and progressive degradation of coacervate for at least 4 weeks *in situ* in infarcted hearts.

Discussion

Molecular therapy using trophic factors to promote cardiac repair and regeneration has been widely investigated [35, 36]. To promote revascularization in the ischemic myocardium, angiogenic GFs such as FGF2 and VEGF have been successfully tested in pre-clinical models of MI [37, 38]. However, clinical attempts using angiogenic GFs have demonstrated mixed results [37]. One major obstacle of molecular therapy with exogenous GFs and/or cytokines is the short *in vivo* half-life of most biological factors. In addition, the bioavailability of systemically delivered trophic factor(s) in the target tissue/organ varies dramatically, highly dependent on the availability of local vasculature. These shortcomings have led to common administrations of large, repetitive doses of GFs in order to achieve therapeutic efficacy, thus increasing the risk of on-target and/or off-target side effects. For example, VEGF can induce nitric oxide-mediated hypotension when a dose over 50 ng/kg/min is administered by intracoronary infusions in patients with myocardial ischemia [39]. To effectively augment the local bioavailability and potency of exogenous trophic factor(s) and minimize the required therapeutic dosage in the context of ischemic insult, a suitable vehicle for sustained, localized delivery is critically needed.

Nevertheless, recent evidence suggest that following AMI, excessive inflammation in response to ischemic myocardial injury leads a detrimental effect on the LV remodelling and increase the chance of HF [6]. In addition, the influence of local inflammatory reactions and immune cells in endogenous tissue repair and regeneration has been established [40]. Consequently, we postulated that spatially and temporally controlled release of an anti-inflammatory/immunomodulatory agent such as IL-10, in combination with an angiogenic GF like FGF2, can synergistically augment endogenous cardiac repair and further improve long-term prognosis following MI.

In the past decade, a number of controlled release platforms have been developed for therapeutic protein delivery, such as hydrogels, micro-/nano-spheres, electrospun/peptide nanofibers, and affinity-based delivery systems [38, 41]. However, many of these delivery systems faced different challenges including large initial burst release, reduced bioactivity of cargo proteins due to the usage of organic solvents, low protein-loading efficiency, and high cost. Recently our group has developed and optimized an inexpensive, biocompatible heparin-based coacervate delivery system that spatially and temporally controls the release of heparin-binding GFs [7]. We have also demonstrated that controlled FGF2 delivery by coacervate induces long-term angiogenesis and vascular stromal cell recruitment in the peri-infarct border zone post-MI [12]. Treatment with FGF2 coacervate reduced peri-infarct inflammation and fibrosis, likely via rapid reestablishment of functional vasculature [12]. However, beneficial effects of FGF2 coacervate within the infarct area were merely marginal. This was likely caused, at least in part, by the harshly inflammatory microenvironment at the ischemic epicenter post-MI. Given the highly versatile loading capability of heparin with any single or multiple heparin-binding trophic factor(s) [7–10, 24], coacervate is deemed suitable for the controlled delivery of FGF2 and IL-10.

In addition to their heparin-binding affinities, proteins may be physically encapsulated through complex coacervation with oppositely charged components (Figure 1A). Black et al.

lately demonstrated that bovine serum albumin (BSA) can be incorporated efficiently into coacervate droplets formed by poly(l-lysine) (PLys) and poly(d/l-glutamic acid) (PGlu) via electrostatic interaction [42]. Moreover, a maximum loading capacity of up to one BSA per PLys/PGlu pair could be achieved via encapsulation while not altering the secondary structure of the cargo protein [42]. These results suggest the involvement of non-affinity based loading during complex coacervation with PEAD and heparin and additional dimension of loading capability beyond affinity-based binding. Nonetheless, future study is deemed necessary to elucidate the role and capacity of non-affinity based loading in heparin-based coacervate.

In the present study, we showed nearly even incorporation and homogeneous distribution of FGF2 and IL-10 within coacervate droplets. FGF2/IL-10 coacervate not only had high loading efficiencies for FGF2 and IL-10 (approximately 98% for both) but also exhibited low initial releases of around 16.1% FGF2 and 12.5% IL-10 in the presence of heparinase during the first 12 hours and relatively linear releases of both factors thereafter throughout 21 days. The seemingly low cumulative release of IL-10 was primarily due to the spontaneous degradation of released IL-10 and molecules trapped in residual coacervate. Coacervate delivery of FGF2 and IL-10 preserved their bioactivities on cardiac stromal cell proliferation *in vitro*. FGF2/IL-10 coacervate sustained HUVEC and hHP proliferation while reducing CF proliferation in general, especially under the inflammatory stress condition. Recently, low molecular weight FGF2 was shown to attenuate human cardiac myofibroblast (hCMF) activation and hCMF-mediated extracellular matrix dysregulation/remodeling after transforming growth factor (TGF)-β1 stimulation, but did not induce hCMF apoptosis [43]. Nevertheless, whether FGF2/IL-10 coacervate also has a role in cellular apoptosis and/or CMF activation in addition to its proliferative impact should be further investigated at the protein level. Moreover, we have tested a stress combination of serum deprivation and hypoxia (2% O_2) to closely simulate an ischemic effect. However, this stress combination appeared to be too harsh and resulted in massive cell death (data not shown), implying a limitation of *in vitro* culture simulation for ischemia. Overall, more research is required to provide mechanistic correlations between the relative dosage/duration of coacervate-based FGF2 and IL-10 delivery and proliferative/apoptotic signaling in different cardiac stromal cell populations.

Hearts treated with FGF2/IL-10 coacervate, Coa-F/I-500/500 in particular, exhibited significantly improved long-term LV contractile function and ameliorated LV dilatation, suggesting the synergistically therapeutic efficacy by controlled delivery of FGF2 and IL-10. FGF2/IL-10 coacervate, especially Coa-F/I-500/500, augmented long-term revascularization, particularly at the infarct area. Our data also imply a positive correlation of revascularizing effects with the dose of IL-10. Whether a reduction of blood vessel loss, a promotion of neovascular growth, or both, played a major role in FGF-2/IL-10-mediated revascularizing benefits after ischemic injury requires future investigation, especially at early time points. In addition, coacervate containing FGF2 and 500 ng IL-10 reduced LV fibrosis, preserved infarct wall thickness, and inhibited chronic phagocytic cell infiltration at the infarct area, more effective than coacervate loaded with FGF2 alone. These results further suggest the synergistic effects of coacervate with FGF2 and IL-10 in anti-fibrosis and

anti-inflammation. Nevertheless, more studies are needed to reveal the effects of coacervate delivered FGF2 and IL-10 on acute inflammatory responses and the phenotype switching of inflammatory cells [6, 44].

Moreover, Coa-F/I-500/100 and Coa-F/I-500/500 had substantially augmented long-term LV myocardial elasticity, maintaining around 80% of the normal myocardial strain. Interestingly, Coa-F-500 treated hearts also exhibited significantly increased myocardial elasticity. These data suggest the primary effect of controlled, localized delivery of FGF2 on myocardial elasticity, largely independent of IL-10 mediated anti-inflammatory benefits. This is likely attributed to the enhanced functional revascularization and reduced cardiomyocyte death mediated by controlled release of FGF2 [12]. Nevertheless, echocardiography in the present study was only performed with a short-axis view. A parasternal long-axis view with measurements of the area and volume change over the entire LV following MI would further enable the quantitative assessment and interpretation of regional and global cardiac function and elasticity in the remodeling murine hearts [45]. Putative mechanisms involved in FGF2/IL-10 coacervate mediated ischemic heart repair have been summarized with a schematic depiction in Supplemental Figure 3.

Previously we have demonstrated that coacervate exhibited a desired spatial distribution in the infarcted myocardium at 3 days post-injection, which is essential for therapeutic protein delivery that targets local tissues [12]. The present estimation of the duration of coacervate treatment post-MI by MPE imaging indicates that injected coacervate had a temporal distribution of at least 4 weeks *in situ*. Consequently, FGF2, IL-10, or other therapeutic proteins with high heparin affinity will likely persist within coacervate and increase their long-term bioavailability in the local tissue. However, future studies with more sensitive approaches are needed to precisely determine the dynamic release of coacervate delivered trophic factors *in vivo*.

Overall, Coa-F/I-500/500 exhibited the highest therapeutic potential among all treatment groups. This warrants the pre-clinical translation of coacervate delivery of FGF2 in combination with IL-10 in large animal models. In addition, the application of FGF2/IL-10 coacervate for the treatment of other ischemic conditions such as myocardial reperfusion injury and peripheral artery disease demands future investigation. Nevertheless, how the different doses of IL-10 are correlated to the therapeutic outcome remains to be further elucidated. Currently we are investigating the dose-dependent effect(s) and the precise mechanism(s) of anti-inflammation and immunomodulation mediated by controlled release of IL-10.

Conclusions

In summary, heparin-based coacervate represents a promising vehicle for localized, controlled delivery of a combination of angiogenic and anti-inflammatory proteins. A single coacervate treatment with 500 ng each of FGF2 and IL-10 resulted in long-term synergistic benefits in a mouse MI model. Future study in pre-clinical large animal models is warranted to evaluate its therapeutic potential for the treating ischemic heart disease. Given that heparin binds a wide range of trophic factors, coacervate delivery of single or multiple

therapeutic proteins can be further expanded to applications in different pathological conditions.

Supplementary Material

Refer to Web version on PubMed Central for supplementary material.

Acknowledgement

The authors sincerely appreciate Greg Gibson, Dr. Simon Watkins, and the Center for Biologic Imaging at the University of Pittsburgh for their expert assistance in multi-photon and confocal microcopy. The authors also wish to thank Scientific Protein Labs for donating clinical-grade heparin and Drs. Jiao Yu and Seunghan Ha for their technical assistance with the ultrasound scanner. This work was supported by grants from the American Heart Association Established Investigator Award 12EIA9020016 (Y.W.), the Henry J. Mankin Endowed Chair (J.H.), and National Institute of Health 1R21EB016774 (J.H.). *In vivo* animal imaging was performed using an ultrasound scanner supported by NIH shared instrument grant NIH1S10RR027383 (K.K.).

Reference

1. Go AS, et al. Executive Summary: Heart Disease and Stroke Statistics—2014 Update: A Report From the American Heart Association. Circulation. 2014; 129(3):399–410. [PubMed: 24446411]
2. Schoen, FJ.; Mitchell, RN. Chapter 12. The Heart. In: Kumar, V., et al., editors. Robbins & Cotran Pathologic Basis of Disease. Philadelphia, PA: Saunders Elsevier; 2010. p. 555-618.
3. Lui KO, Zangi L, Chien KR. Cardiovascular regenerative therapeutics via synthetic paracrine factor modified mRNA. Stem Cell Research. 2014; 13(3, Part B):693–704. [PubMed: 25043723]
4. Qian L, et al. In vivo reprogramming of murine cardiac fibroblasts into induced cardiomyocytes. Nature. 2012; 485(7400):593–598. [PubMed: 22522929]
5. Senyo SE, Lee RT, Kühn B. Cardiac regeneration based on mechanisms of cardiomyocyte proliferation and differentiation. Stem Cell Research. 2014; 13(3, Part B):532–541. [PubMed: 25306390]
6. Latet SC, et al. The cellular immune system in the post-myocardial infarction repair process. International Journal of Cardiology. 2015; 179(0):240–247. [PubMed: 25464457]
7. Chu H, et al. A [polycation:heparin] complex releases growth factors with enhanced bioactivity. Journal of Controlled Release. 2011; 150(2):157–163. [PubMed: 21118705]
8. Johnson NR, Wang Y. Controlled delivery of heparin-binding EGF-like growth factor yields fast and comprehensive wound healing. Journal of Controlled Release. 2013; 166(2):124–129. [PubMed: 23154193]
9. Lee K-W, et al. Human progenitor cell recruitment via SDF-1α coacervate-laden PGS vascular grafts. Biomaterials. 2013; 34(38):9877–9885. [PubMed: 24060423]
10. Li H, et al. Sustained Release of Bone Morphogenetic Protein 2 via Coacervate Improves the Osteogenic Potential of Muscle-Derived Stem Cells. Stem Cells Translational Medicine. 2013; 2(9):667–677. [PubMed: 23884640]
11. Chu H, et al. Injectable fibroblast growth factor-2 coacervate for persistent angiogenesis. Proceedings of the National Academy of Sciences. 2011; 108(33):13444–13449.
12. Chu H, et al. The effect of a heparin-based coacervate of fibroblast growth factor-2 on scarring in the infarcted myocardium. Biomaterials. 2013; 34(6):1747–1756. [PubMed: 23211448]
13. Moore KW, et al. INTERLEUKIN-10 AND THE INTERLEUKIN-10 RECEPTOR. Annual Review of Immunology. 2001; 19(1):683–765.
14. Salek-Ardakani S, et al. Heparin and heparan sulfate bind interleukin-10 and modulate its activity. Blood. 2000; 96(5):1879–1888. [PubMed: 10961890]
15. Frangogiannis NG. Regulation of the Inflammatory Response in Cardiac Repair. Circulation Research. 2012; 110(1):159–173. [PubMed: 22223212]
16. Gullestad L, et al. Immunomodulating Therapy With Intravenous Immunoglobulin in Patients With Chronic Heart Failure. Circulation. 2001; 103(2):220–225. [PubMed: 11208680]

17. Stumpf C, et al. Interleukin-10 improves left ventricular function in rats with heart failure subsequent to myocardial infarction. European Journal of Heart Failure. 2008; 10(8):733–739. [PubMed: 18599346]
18. Huhn RD, et al. Pharmacodynamics of subcutaneous recombinant human interleukin-10 in healthy volunteers[ast]. Clin Pharmacol Ther. 1997; 62(2):171–180. [PubMed: 9284853]
19. Madduri S, et al. Effect of controlled co-delivery of synergistic neurotrophic factors on early nerve regeneration in rats. Biomaterials. 2010; 31(32):8402–8409. [PubMed: 20692034]
20. Kim SE, et al. Co-delivery of platelet-derived growth factor (PDGF-BB) and bone morphogenic protein (BMP-2) coated onto heparinized titanium for improving osteoblast function and osteointegration. Journal of Tissue Engineering and Regenerative Medicine. 2013 [Epub ahead of print].
21. Banquet S, et al. Arteriogenic Therapy by Intramyocardial Sustained Delivery of a Novel Growth Factor Combination Prevents Chronic Heart Failure. Circulation. 2011; 124(9):1059–1069. [PubMed: 21824923]
22. Kim JH, et al. The enhancement of mature vessel formation and cardiac function in infarcted hearts using dual growth factor delivery with self-assembling peptides. Biomaterials. 2011; 32(26):6080–6088. [PubMed: 21636123]
23. Shin S-H, et al. Co-delivery of Vascular Endothelial Growth Factor and Angiopoietin-1 Using Injectable Microsphere/Hydrogel Hybrid Systems for Therapeutic Angiogenesis. Pharmaceutical Research. 2013; 30(8):2157–2165. [PubMed: 23686375]
24. Awada HK, Johnson NR, Wang Y. Dual Delivery of Vascular Endothelial Growth Factor and Hepatocyte Growth Factor Coacervate Displays Strong Angiogenic Effects. Macromolecular Bioscience. 2014; 14(5):679–686. [PubMed: 24452960]
25. Chu H, Gao J, Wang Y. Design, synthesis, and biocompatibility of an arginine-based polyester. Biotechnology Progress. 2012; 28(1):257–264. [PubMed: 22034156]
26. Balasubramanian S, et al. β3 Integrin in Cardiac Fibroblast Is Critical for Extracellular Matrix Accumulation during Pressure Overload Hypertrophy in Mouse. PLoS ONE. 2012; 7(9):e45076. [PubMed: 22984613]
27. Chen WCW, et al. Human Myocardial Pericytes: Multipotent Mesodermal Precursors Exhibiting Cardiac Specificity. STEM CELLS. 2015; 33(2):557–573. [PubMed: 25336400]
28. Chen C-W, et al. Human Pericytes for Ischemic Heart Repair. STEM CELLS. 2013; 31(2):305–316. [PubMed: 23165704]
29. Manning WJ, et al. In vivo assessment of LV mass in mice using high-frequency cardiac ultrasound: necropsy validation. American Journal of Physiology - Heart and Circulatory Physiology. 1994; 266(4):H1672–H1675.
30. Pollick C, Hale SL, Kloner RA. Echocardiographic and cardiac doppler assessment of mice. Journal of the American Society of Echocardiography. 1995; 8(5, Part 1):602–610. [PubMed: 9417202]
31. Wandt B, et al. Echocardiographic assessment of ejection fraction in left ventricular hypertrophy. Heart. 1999; 82(2):192–198. [PubMed: 10409535]
32. O'Donnell M, et al. Internal displacement and strain imaging using ultrasonic speckle tracking. Ultrasonics, Ferroelectrics, and Frequency Control, IEEE Transactions on. 1994; 41(3):314–325.
33. Lubinski MA, Emelianov SY, O'Donnell M. Speckle tracking methods for ultrasonic elasticity imaging using short-time correlation. Ultrasonics, Ferroelectrics, and Frequency Control, IEEE Transactions on. 1999; 46(1):82–96.
34. Kinsella L, et al. Interactions of putative heparin-binding domains of basic fibroblast growth factor and its receptor, FGFR-1, with heparin using synthetic peptides. Glycoconjugate Journal. 1998; 15(4):419–422. [PubMed: 9613830]
35. Nagai T, Komuro I. Gene and cytokine therapy for heart failure: molecular mechanisms in the improvement of cardiac function. 2012; Vol. 303:H501–H512.
36. Hastings CL, et al. Drug and cell delivery for cardiac regeneration. Advanced Drug Delivery Reviews. 2014 [Epub ahead of print].
37. Segers VM, Lee R. Protein Therapeutics for Cardiac Regeneration after Myocardial Infarction. Journal of Cardiovascular Translational Research. 2010; 3(5):469–477. [PubMed: 20607468]

38. Chu H, Wang Y. Therapeutic angiogenesis: controlled delivery of angiogenic factors. Therapeutic Delivery. 2012; 3(6):693–714. [PubMed: 22838066]

39. Henry TD, et al. Intracoronary administration of recombinant human vascular endothelial growth factor to patients with coronary artery disease. American Heart Journal. 2001; 142(5):872–880. [PubMed: 11685177]

40. Forbes SJ, Rosenthal N. Preparing the ground for tissue regeneration: from mechanism to therapy. Nat Med. 2014; 20(8):857–869. [PubMed: 25100531]

41. Mohtaram NK, Montgomery A, Willerth SM. Biomaterial-based drug delivery systems for the controlled release of neurotrophic factors. Biomedical Materials. 2013; 8(2):022001. [PubMed: 23385544]

42. Black KA, et al. Protein Encapsulation via Polypeptide Complex Coacervation. ACS Macro Letters. 2014; 3(10):1088–1091.

43. Svystonyuk DA, et al. Fibroblast growth factor-2 regulates human cardiac myofibroblast-mediated extracellular matrix remodeling. Journal of Translational Medicine. 2015; 13:147. [PubMed: 25948488]

44. Pinto AR, Godwin JW, Rosenthal NA. Macrophages in cardiac homeostasis, injury responses and progenitor cell mobilisation. Stem Cell Research. 2014; 13(3, Part B):705–714. [PubMed: 25087895]

45. Bhan A, et al. High-frequency speckle tracking echocardiography in the assessment of left ventricular function and remodeling after murine myocardial infarction. 2014; Vol. 306:H1371–H1383.

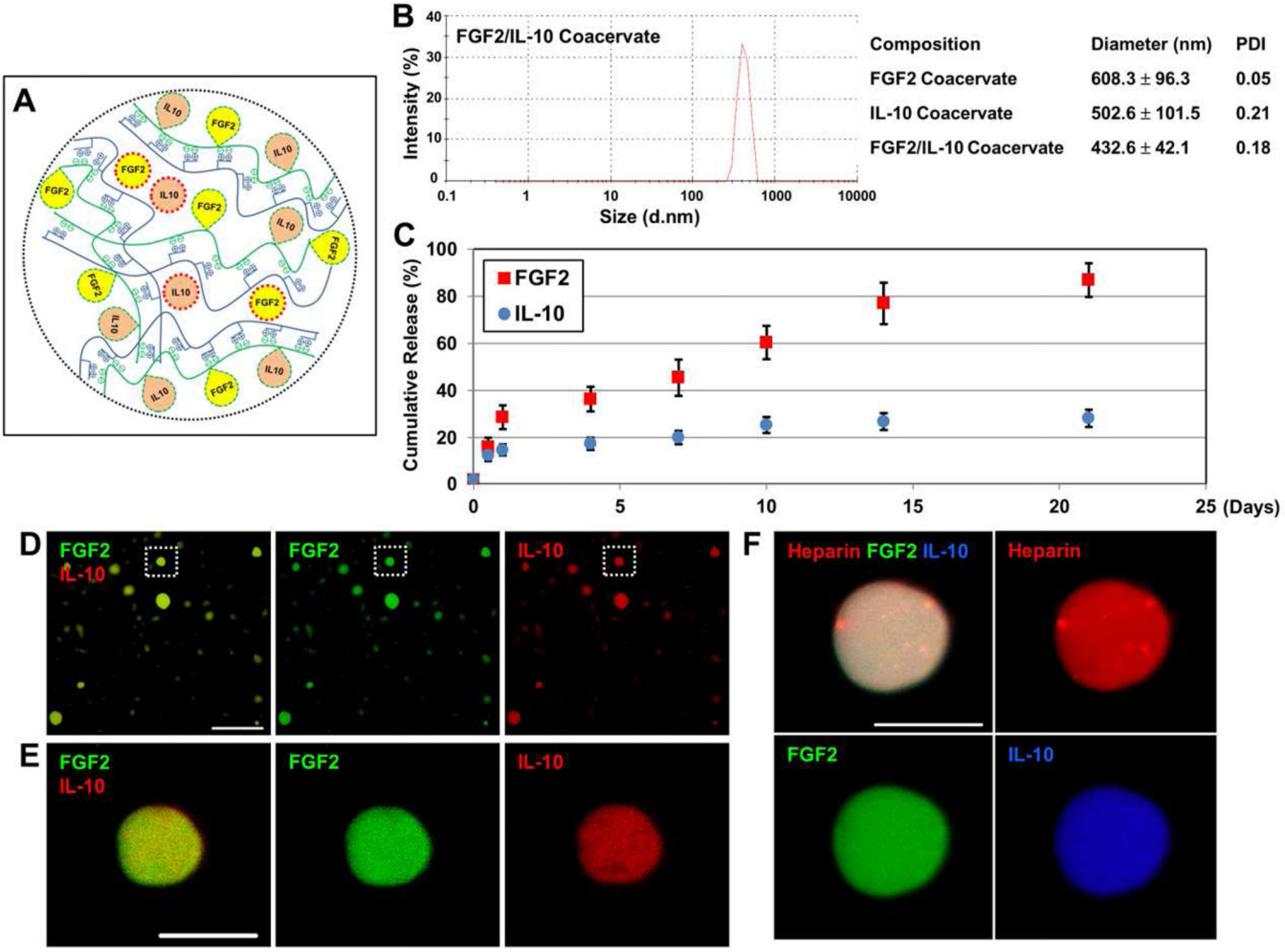

Figure 1. Characterization of FGF2/IL-10 coacervate

(A) Schematic illustration of putative FGF2/IL-10 coacervate structure (PEAD in blue, heparin in green, FGF2 in yellow, and IL-10 in orange). Please note that FGF2 and IL-10 molecules bound to heparin are circled with green dashed lines while FGF2 and IL-10 molecules physically entrapped within the coacervate structure (no affinity-based binding) are circled with red dashed line. (B) Analysis of coacervate droplet size with polydispersity index (PDI). (C) The release profile of FGF2/IL-10 coacervate *in vitro* for 3 weeks. Equal amount of FGF2 and IL-10 were first combined and then mixed with heparin, followed by the addition of PEAD to form coacervate, with a mass ratio of PEAD:heparin:FGF2:IL-10=500:100:1:1. Supernatants were collected on Day 0, 0.5, 1, 4, 7, 10, 14, and 21 and then replenished with PBS containing fresh 0.5 U/mL heparinase II in order to simulate the release of cargo proteins *in vivo* (N=4 per time point). The amount of released FGF2 and IL-10 was measured by ELISA. Data are presented as percent cumulative release (normalized to the original load). Error bars indicate means ± SD. (D) Incorporation of fluorescently labeled FGF2 (green) and IL-10 (red) into coacervate droplets (scale bar = 25 μm) (E) High-magnification enlargement of the coacervate droplet in the dotted area in (D) showing fluorescently labeled FGF-2 and IL-10 molecules evenly distributed within the droplet (scale bar = 5 μm). (F) Triply labeled heparin (red), FGF2

(green) and IL-10 (blue) showing nearly homogeneous structure of FGF-2/IL-10 coacervate (scale bar = 10 μm). Please note that due to the limitation of imaging resolution, larger coacervate droplets were chosen for high-magnification imaging.

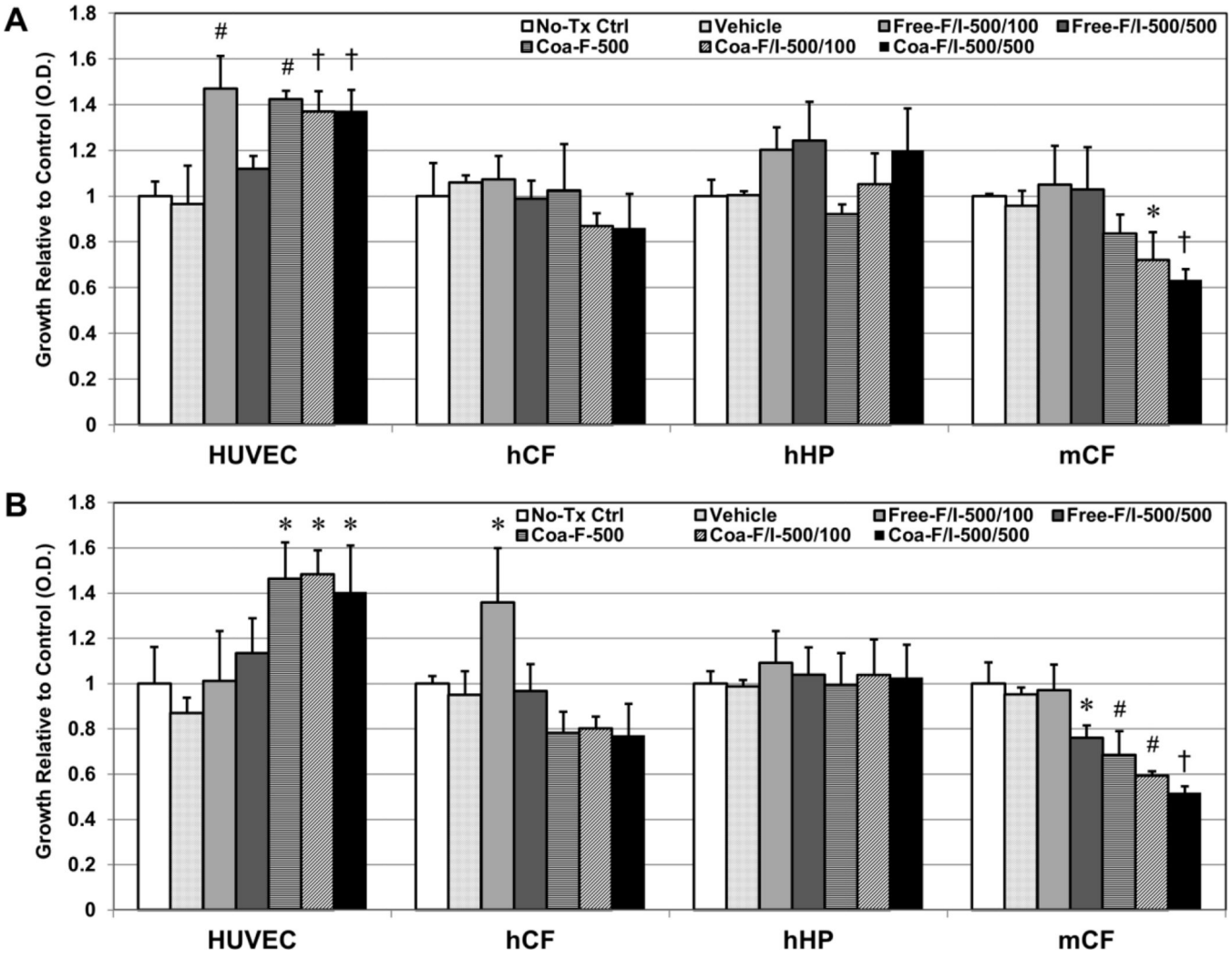

Figure 2. Bioactivity of FGF-2/IL-10 coacervate on cardiac stromal cell proliferation *in vitro*

Bioactivity of FGF2/IL-10 coacervate on cardiac stromal cell proliferation was tested in a non-contact transwell system for 72 hours with human umbilical vein endothelial cells (HUVECs), human cardiac fibroblasts (hCFs), and human heart pericytes (hHPs), and mouse cardiac fibroblasts (mCFs) cultured at bottom wells and treatment solutions loaded into suspended transwells. (A) Under the simple serum-deprived condition, Free-F/I-500/100, Coa-F-500, Coa-F/I-500/100 and Coa-F/I-500/500 had significantly higher HUVEC proliferation than the no-treatment control and Free-F/I-500/500. Coa-F/I-500/500 had significantly lower mCF proliferation than the no-treatment control, Free-F/I-500/100, and Free-F/I-500/500 while Coa-F/I-500/100 had significantly lower mCF proliferation than Free-F/I-500/100 and Free-F/I-500/500. Free-F/I-500/100, Free-F/I-500/500, and Coa-F/I-500/500 marginally promoted hHP proliferation (all $p>0.05$). (B) Under the serum-deprived condition with inflammatory stress (10 ng/ml of TNF-α for HUVECs and 100 ng/ml of TNF-α for all other cell types), Coa-F-500, Coa-F/I-500/100, and Coa-F/I-500/500 had significantly higher HUVEC proliferation than the no-treatment control. Coa-F-500, Coa-F/I-500/100, and Coa-F/I-500/500 had significantly lower hCF proliferation than Free-

F/I-500/100. Additionally, Coa-F/I-500/500 had significantly lower mCF proliferation than the no-treatment control, Free-F/I-500/100, and Free-F/I-500/500 while Coa-F-500 and Coa-F/I-500/100 had significantly lower mCF proliferation than the no-treatment control and Free-F/I-500/100. Error bars indicate means ± SD. Statistical differences between groups were analyzed by one-way ANOVA with Bonferroni post-hoc analysis. (*$p \leq 0.05$, $^{\dagger}p \leq 0.01$, $^{\S}p \leq 0.005$, $^{\#}p \leq 0.001$ in all graphs) (No-Tc Ctrl: basal medium; Vehicle: empty [PEAD:heparin] coacervate; Free-F/I-500/100: naked mixture of 500 ng FGF2 and 100 ng IL-10; Free-F/I-500/500: naked mixture of 500 ng FGF2 and 500 ng IL-10; Coa-F-500: coacervate loaded with 500 ng FGF2; Coa-F/I-500/100: coacervate loaded with 500 ng FGF2 and 100 ng IL-10; Coa-F/I-500/500: coacervate loaded with 500 ng FGF2 and 500 ng IL-10)

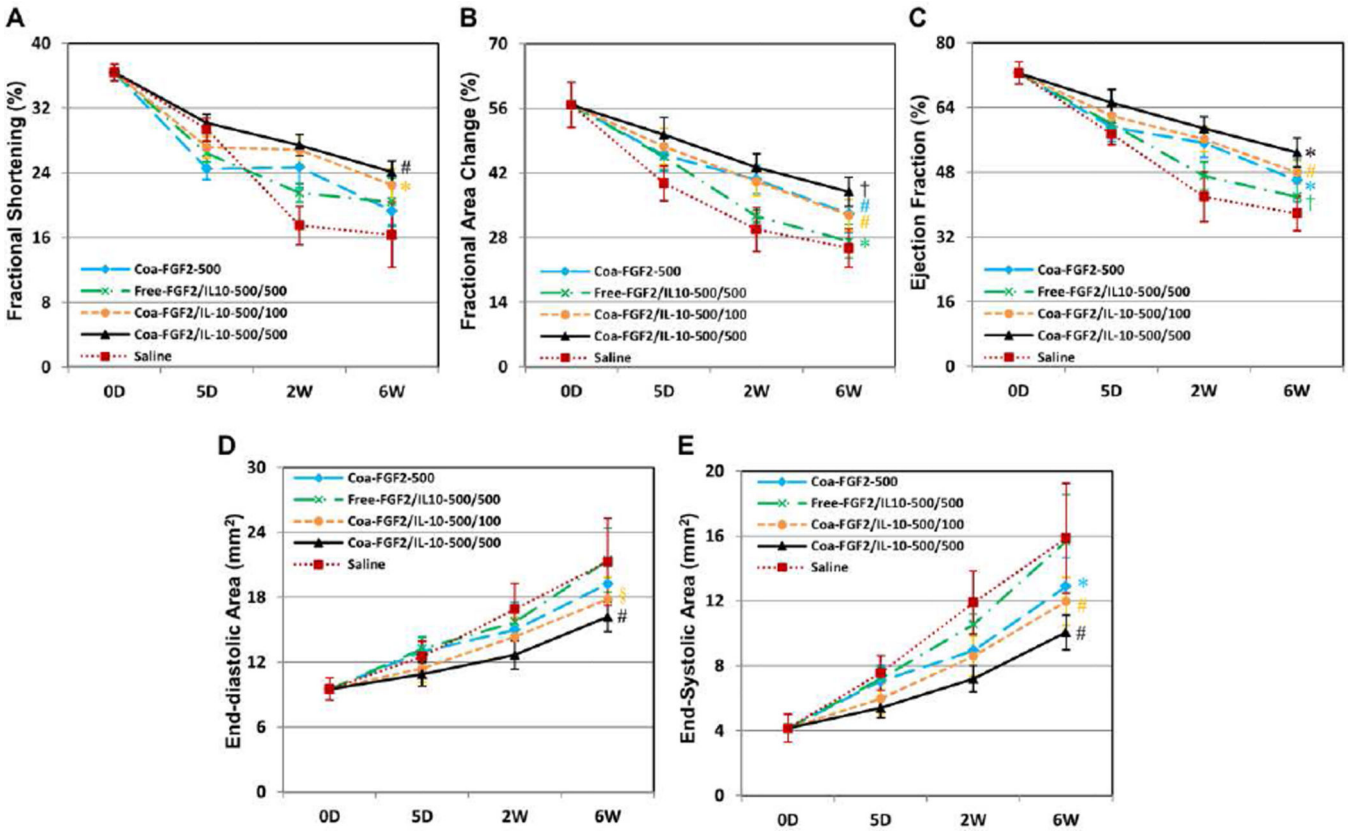

Figure 3. Intramyocardial injection of FGF2/IL-10 coacervate improves long-term cardiac contractility and ameliorates adverse remodeling

Echocardiographic analyses (N=8 per group except Free-F/I-500/500, N=7) were repeatedly performed at 5 days, 2 and 6 weeks post-surgery. Statistical differences in overall treatment effect were analyzed by two-way repeated ANOVA with Bonferroni multiple comparison test. The results revealed substantial improvement in LV contractility following intramyocardial injection of either Coa-F/I-500/100 or Coa-F/I-500/500, as indicated by the higher (A) fractional shortening (FS), (B) fractional area change (FAC), and (C) ejection fraction (EF) (*$p \leq 0.05$, $^{\dagger}p \leq 0.01$, $^{\S}p \leq 0.005$, $^{\#}p \leq 0.001$ in all graphs; FS: Coa-F/I-500/100 and Coa-F/I-500/500 vs. Saline, Free-F/I-500/500, and Coa-F-500; FAC and EF: Coa-F/I-500/500 vs. all groups, Coa-F-500 and Coa-F/I-500/100 vs. Saline and Free-F/I-500/500, Free-F/I-500/500 vs. Saline). Significant reductions of (D) end-diastolic area (EDA) and (E) end-systolic area (ESA) of LV were observed in hearts treated with Coa-F/I-500/100 or Coa-F/I-500/500 (*$p \leq 0.05$, $^{\dagger}p \leq 0.01$, $^{\S}p \leq 0.005$, $^{\#}p \leq 0.001$ in all graphs; EDA: Coa-F/I-500/500 vs. Saline, Free-F/I-500/500, and Coa-F-500; Coa-F/I-500/100 vs. Saline and Free-F/I-500/500; ESA: Coa-F/I-500/500 vs. Saline, Free-F/I-500/500, and Coa-F-500; Coa-F-500 and Coa-F/I-500/100 vs. Saline and Free-F/I-500/500). Error bars indicate means ± SD. Please note that time points on the X-axis (time) in all graphs are not scaled to actual experimental duration.

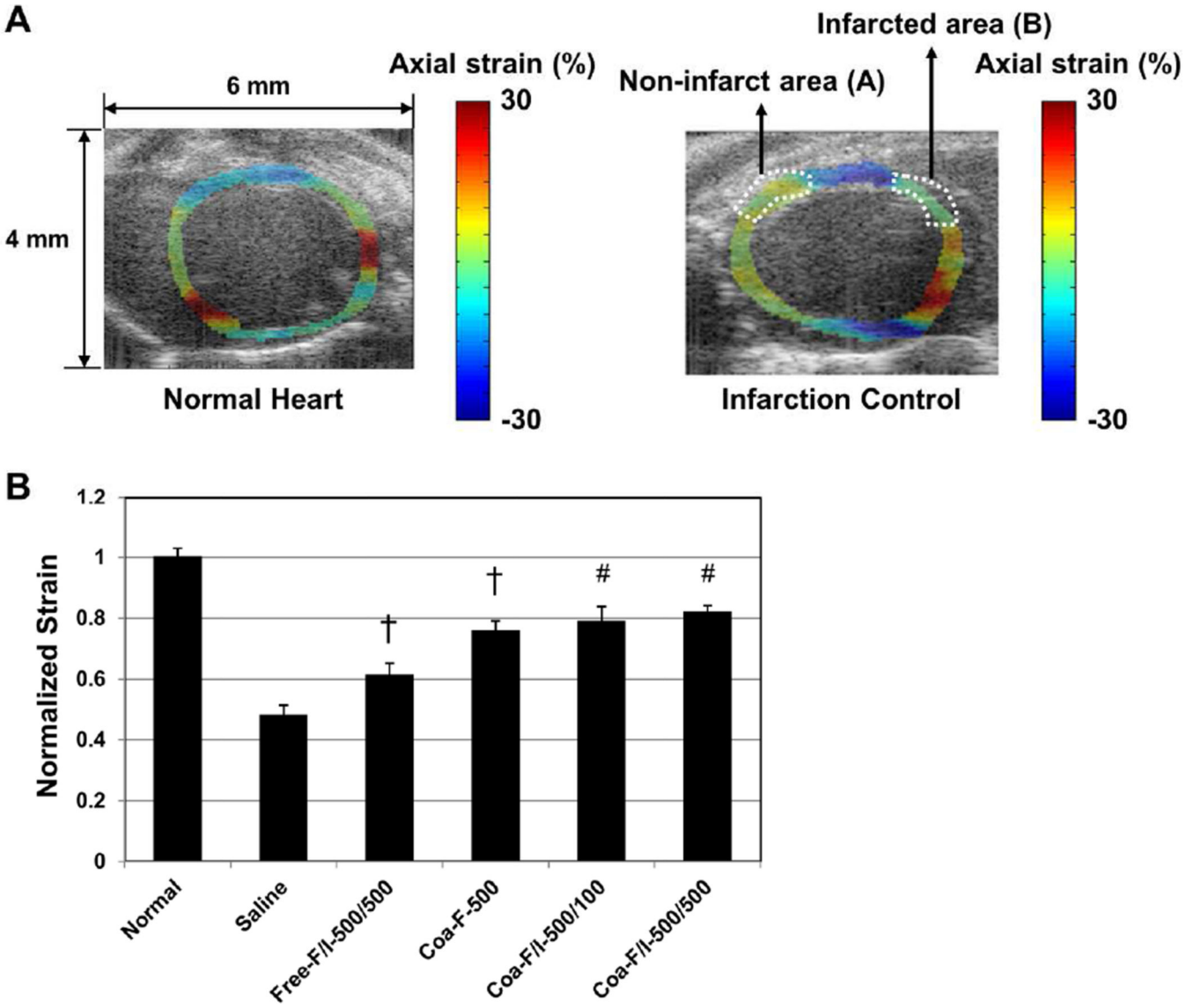

Figure 4. FGF-2/IL-10 coacervate amends elasticity of infarcted myocardium

(A) Representative axial strain maps laid over B-mode images (4 × 6 mm) showing the axial strain distribution of the normal (left panel) and untreated MI control (right panel, mid-infarct level) left ventricles respectively. For normalization purpose, the infarct area was designated as B, and the non-infarct area was designated as A. (B) Normalized strain was obtained by dividing spatially averaged axial strain of B by that of A (B/A). Coa-F-500, Coa-F/I-500/100, and Coa-F/I-500/500 showed markedly greater normalized strains than the saline control and Free-F/I-500/500. Free-F/I-500/500 also showed notably higher normalized strains than the saline control ($^{\#}p \leq 0.001$, $^{\dagger}p \leq 0.01$; N=3 per group). Error bars indicate means ± SD. Statistical differences between groups were analyzed by one-way ANOVA with Bonferroni post-hoc analysis.

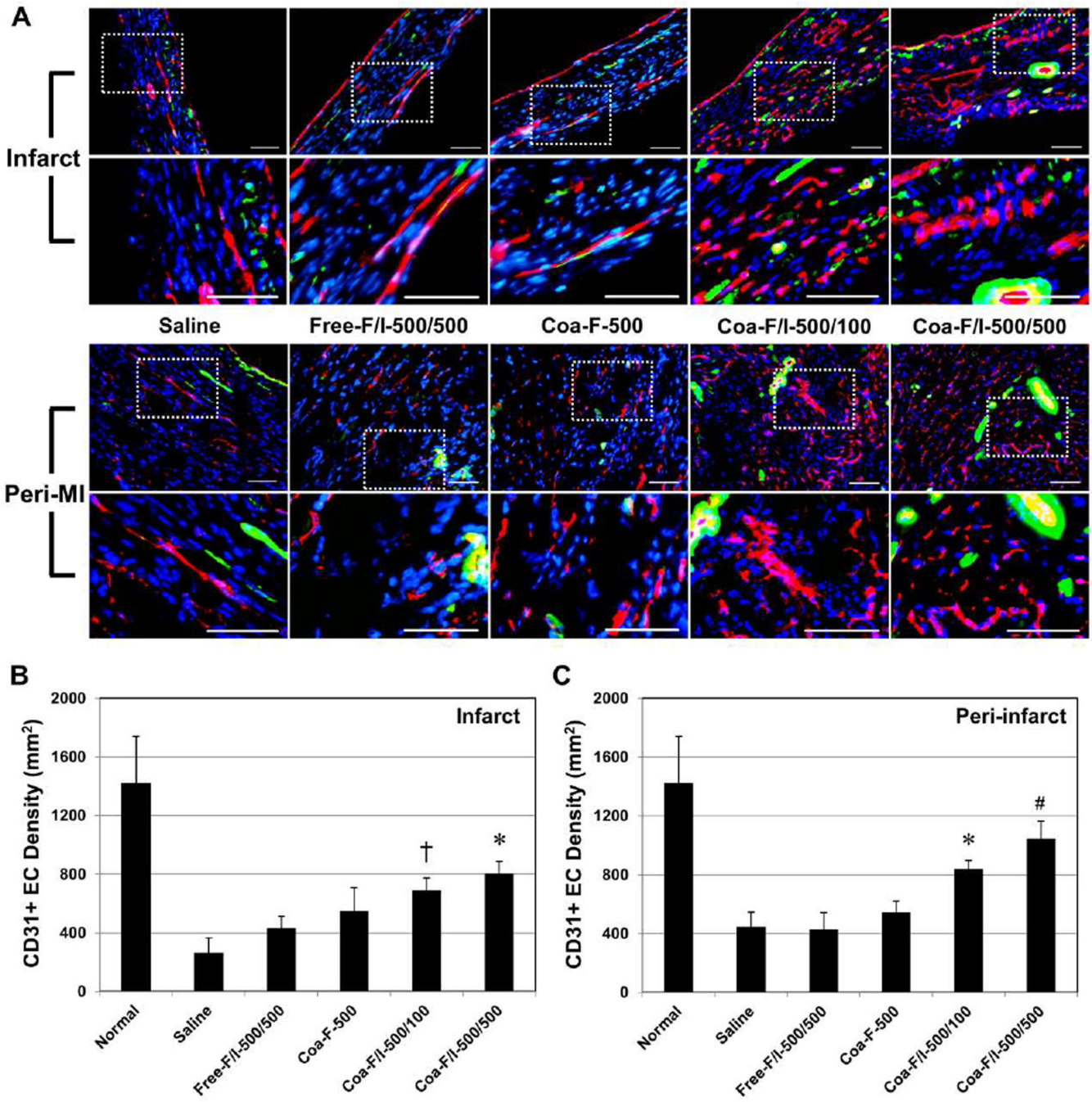

Figure 5. FGF-2/IL-10 coacervate increases long-term endothelial cell density

Endothelial cell (EC) density at the infarct and peri-infarct border zone was revealed by immunohistochemical detection of CD31+ ECs at 6 weeks post-infarction. (A) Representative images of CD31+ ECs (red) and aSMA+ cells (green) within the infarct and peri-infarct areas at the mid-infarct level, with dotted areas enlarged. Please note that vascular smooth muscle cells (VSMC) were defined as perivascular/peri-CD31 aSMA+ cells. Nuclei were stained with DAPI in blue. (scale bars = 100 mm) (B) Quantitative analyses of CD31+ EC density within the infarct area revealed that Coa-F/I-500/500 had

significantly higher EC density than the saline control and Free-F/I-500/500 while Coa-F/I-500/100 had significantly higher EC density than the saline control (*$p \leq 0.05$, $^{\dagger}p \leq 0.01$; N=4 per group). (C) Within the peri-infarct area, Coa-F/I-500/500 had significantly higher EC density than the saline control, Free-F/I-500/500, and Coa-F-500 while Coa-F/I-500/100 had significantly higher EC density than the saline control and Free-F/I-500/500 ($^{\#}p \leq 0.001$, *$p \leq 0.05$; N=4 per group). Error bars indicate means ± SD. Statistical differences between groups were analyzed by one-way A NOVA with Bonferroni post-hoc analysis.

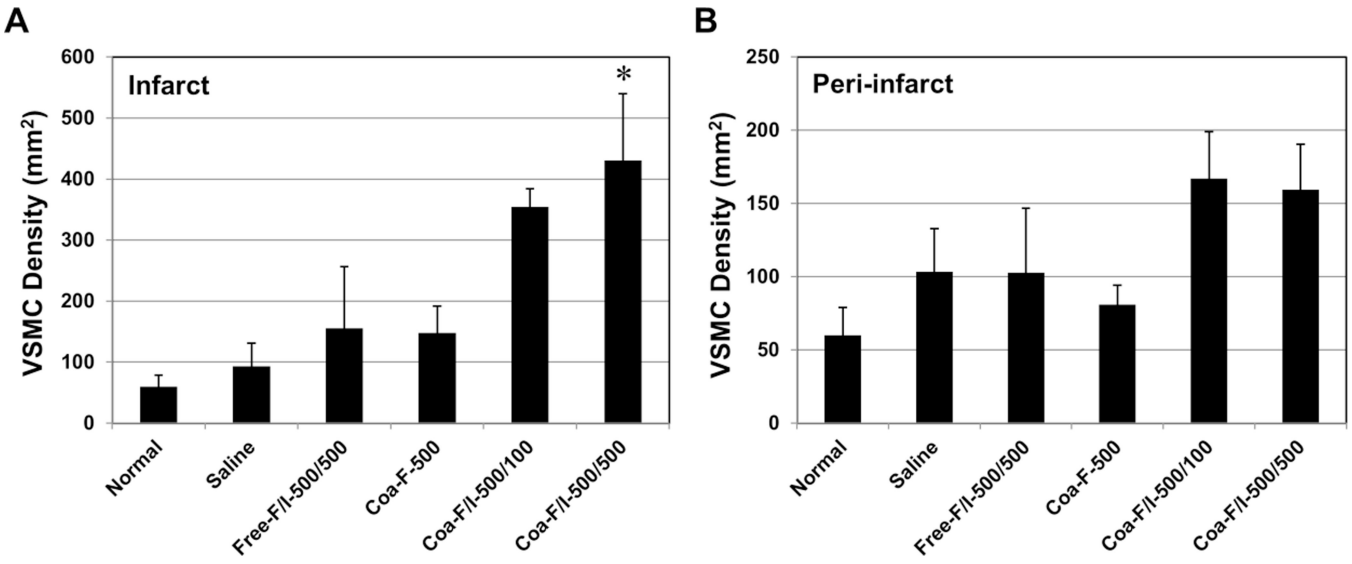

Figure 6. FGF-2/IL-10 coacervate enhances long-term vascular stromal cell density

Vascular stromal cell density at the infarct and peri-infarct border zone was revealed by immunohistochemical detection of vascular smooth muscle cells (VSMC, defined as perivascular/peri-CD31 αSMA+ cells; representative images shown in Figure 5A) at 6 weeks post-infarction. (A) Quantitative analyses of perivascular aSMA+ VSMC density within the infarct area revealed that Coa-F/I-500/500 had significantly higher VSMC density than the saline control, Free-F/I-500/500, and Coa-F-500 (*$p \leq 0.05$; N=4 per group). (B) Coa-F/I-500/100 and Coa-F/I-500/500 had marginally higher VSMC density than the saline control, Free-F/I-500/500, and Coa-F-500 within the peri-infarct area (all $p > 0.05$; N=4 per group). Error bars indicate means ± SD. Statistical differences between groups were analyzed by one-way ANOVA with Bonferroni post-hoc analysis.

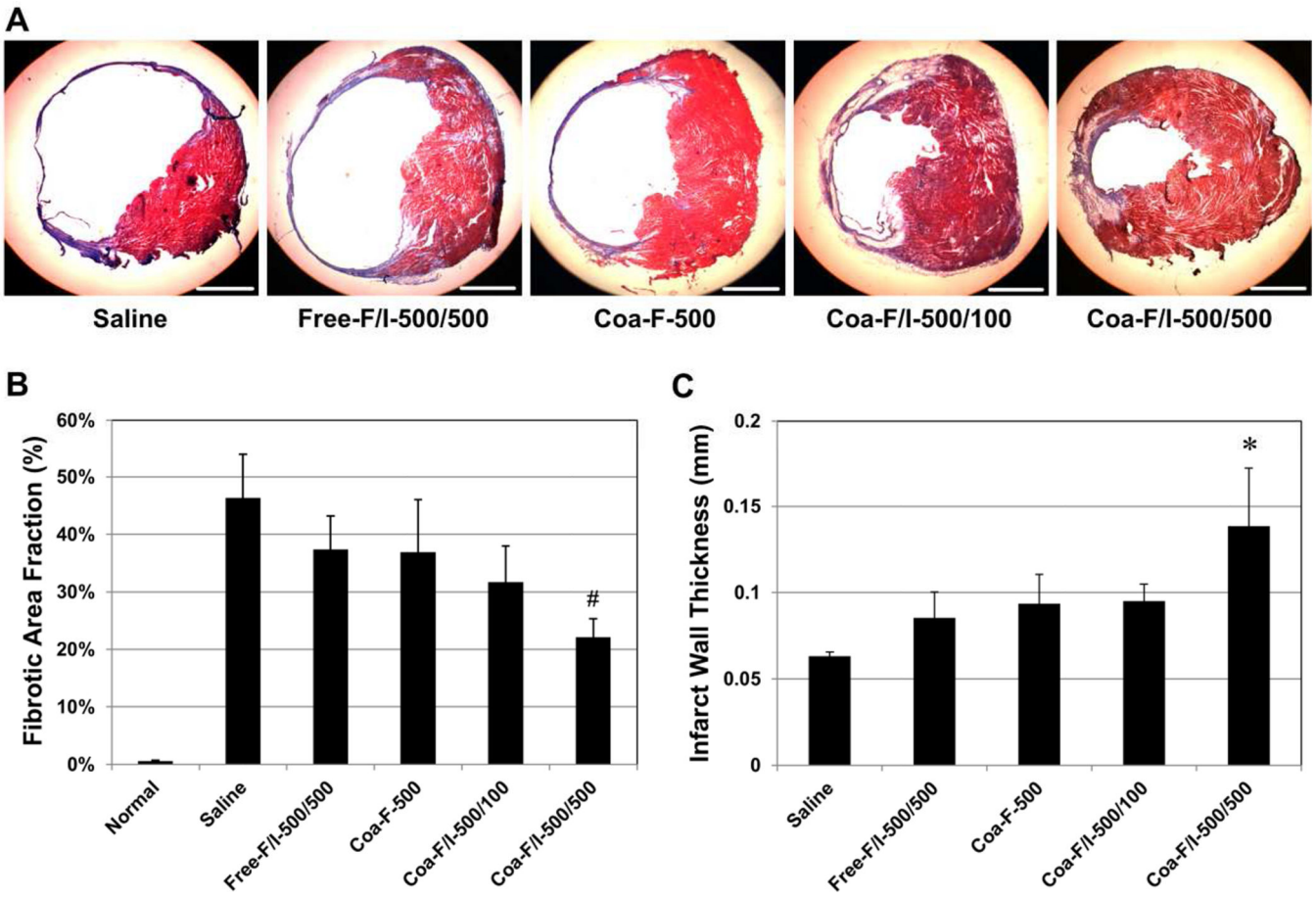

Figure 7. FGF-2/IL-10 coacervate reduces myocardial fibrosis

Masson's trichrome histological staining was employed to reveal left ventricular (LV) myocardial fibrosis at 6 weeks post-infarction. (A) Representative images of myocardial fibrosis at the mid-infarct level (transverse sections of hearts). Collagen deposition (fibrosis/scar) was stained in blue/purple while cardiac muscle was stained in red (scale bars = 1 mm). (B) Quantification of the LV fibrotic area fraction. Coa-F/I-500/500 exhibited significantly reduced LV fibrotic area fraction ($^{\#}p \leq 0.001$, vs. saline; N=4 per group). Healthy heart (Normal) served as a negative control. (C) Measurement of LV wall thickness at the center of the infarct. Coa-F/I-500/500 had significantly thicker infarct wall than all other groups ($^{*}p \leq 0.05$, vs. all groups; N=4 per group). Error bars indicate means ± SD. Statistical differences between groups were analyzed by one-way ANOVA with Bonferroni post-hoc analysis.

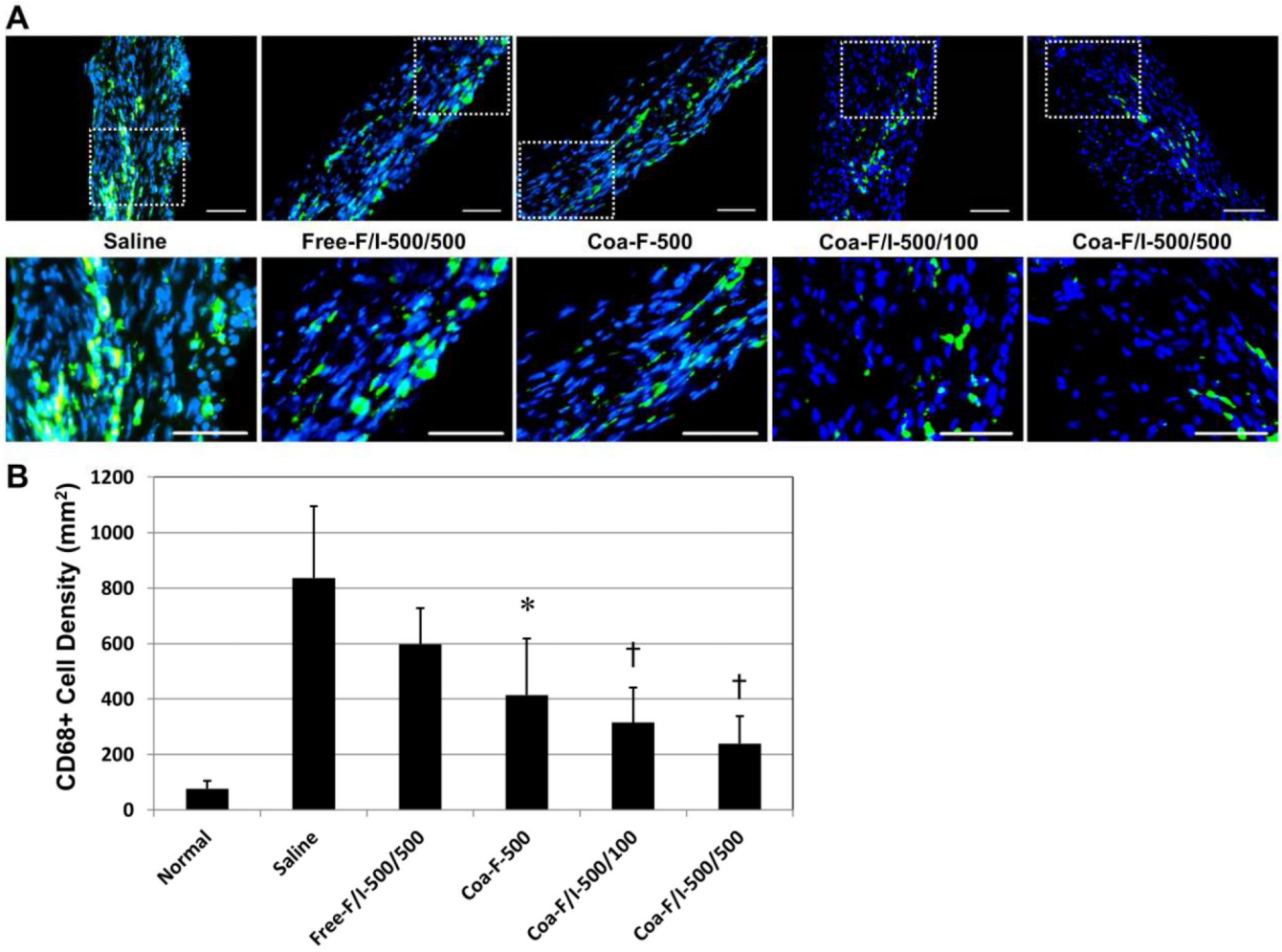

Figure 8. FGF-2/IL-10 coacervate inhibits chronic phagocytic cell infiltration

The effect of FGF-2/IL-10 coacervate on chronic inflammatory responses was evaluated by the number of focally infiltrating CD68+ phagocytic cells within the infarct region at 6 weeks post-infarction. (A) Representative immunofluorescent images of CD68+ cell (green) infiltration within the infarct area at the mid-infarct level, with dotted areas enlarged. Nuclei were stained with DAPI in blue. (scale bars = 100 mm) (B) When compared with the saline control, Coa-F-500, Coa-F/I-500/100, and Coa-F/I-500/500 had significantly reduced numbers of infiltrated CD68+ phagocytic cells within the infarct area. Error bars indicate means ± SD. Statistical differences between groups were analyzed by one-way ANOVA with Bonferroni post-hoc analysis. (*$p \leq 0.05$, $^{\dagger}p \leq 0.01$, vs. saline; N=4 per group)

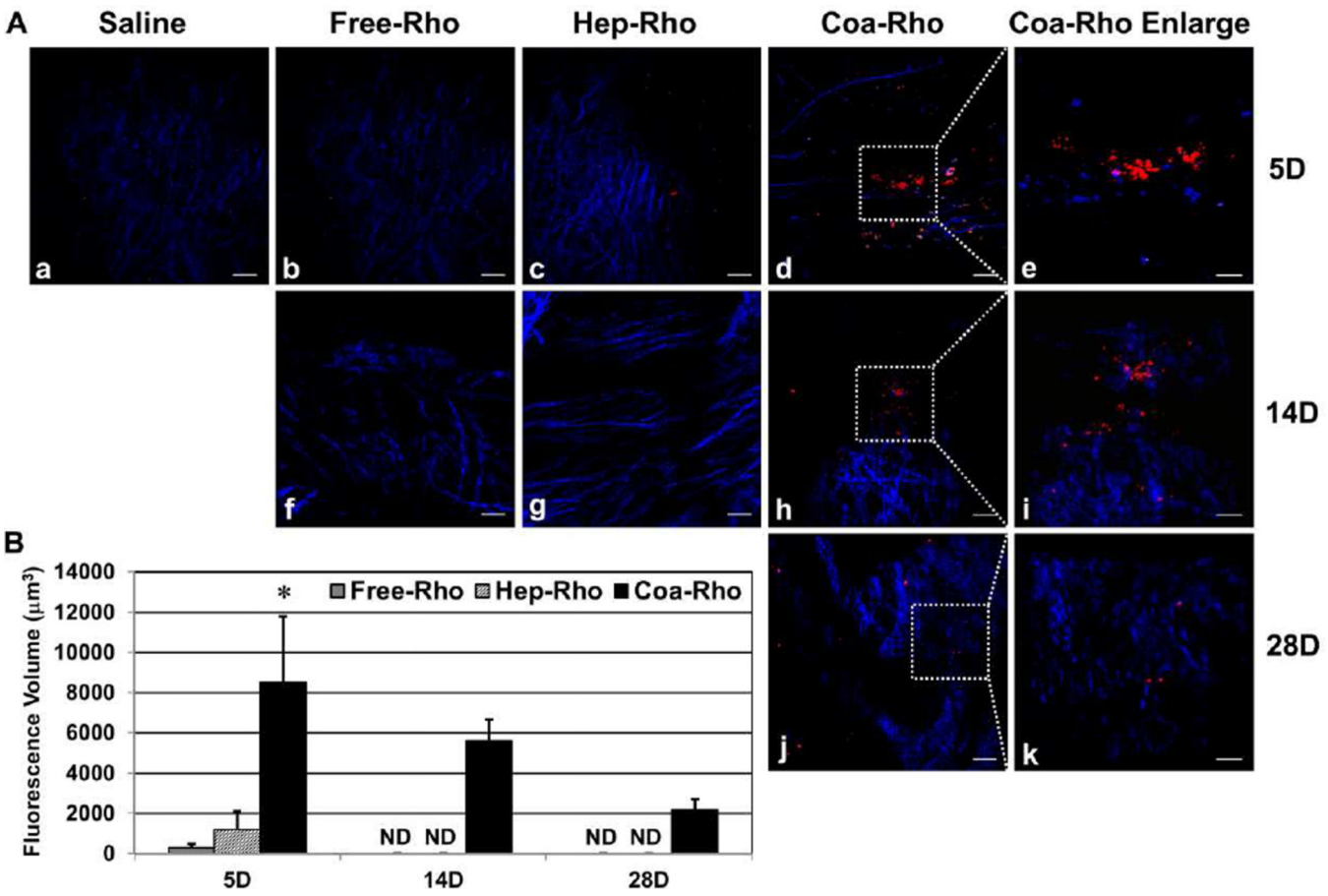

Figure 9. Estimation of the duration of coacervate treatment *in vivo*

Multi-photon excitation (MPE) imaging was employed to detect intramyocardially injected free (Free-Rho), heparin-bound (Hep-Rho), or coacervate-bound rhodamine (Coa-Rho). Collagen fibers (blue) were revealed by second harmonic generation (SHG) signals. (A) Representative MPE images within the infarct area of ischemic hearts injected with saline (a), Free-Rho (b, f), Hep-Rho (c, g), or Coa-Rho (d, h, j) with enlargement of Coa-Rho fluorescent signals within the dotted area in (e), (i), and (k) respectively at 5 (a–e), 14 (f–i), an 28 (j–k) days post-injection (scale bars: (a–d), (f–h), and (j) = 50 μm; (e), (i), and (k) = 20 μm). (B) Quantification of the fluorescence volume of Free-Rho, Hep-Rho, and Coa-Rho at 5, 14, and 28 days post-injection. Error bars indicate means ± SD. Statistical differences between groups were analyzed by one-way ANOVA with Bonferroni post-hoc analysis. (*p<0.05, vs. Free-Rho and Hep-Rho; N=3 per group).